Advanced Materials Science and Technology Vol 6 Issue 1 2024
DOI: 10.37155/2717–526X–0601–5

Review

Open Access

Omniscient Pte.Ltd.

A Review of Mechanical Characterization Techniques for Ultrathin Films Beyond Two-dimensional Materials

Yunfeng Yan[1*], Jiayi He[2], Wenqi Ji[3], Zhuorui Hu[4], Jiaying Xiao[5], Changlin Li[5], Hongxi He[5], Ximing Wang[6], Jiawen Xu[7], Yuxuan Gong[8], Nanlong Sun[9]

[1]State Key Laboratory of Solid Lubrication, Lanzhou Institute of Chemical Physics, Chinese Academy of Sciences, Lanzhou 730000, China
[2]Shien-Ming Wu School of Intelligent Engineering, South China University of Technology, Guangzhou 510641, China
[3]Emergency Management College, Nanjing University of Information Science & Technology, Nanjing 210044, China
[4]School of Microelectronics, South China University of Technology, Guangzhou 510641, China
[5]School of Material Science and Engineering, South China University of Technology, Guangzhou 510641, China
[6]School of Electronic and Information Engineering, Nanjing University of Information Science & Technology, Nanjing 210044, China
[7]Key Laboratory for Liquid-Solid Structural Evolution and Processing of Materials (Ministry of Education), Shandong University, Jinan 250061, China
[8]School of Mechanical and Power Engineering, Jiangsu University Jingjiang College, Zhenjiang 212028, China
[9]School of Agricultural Engineering, Jiangsu University, Zhenjiang 212013, China

***Correspondence to:** Yunfeng Yan, State Key Laboratory of Solid Lubrication, Lanzhou Institute of Chemical Physics, Chinese Academy of Sciences, Lanzhou 730000, China. Email: yunfeng.yan@mail.mcgill.ca

Received: April 17, 2024; **Accept:** June 4, 2024; **Published Online:**

Citation: Yan YF, He JY, Ji WQ, Hu ZR, Xiao JY, Li CL, He HX, Wang XM, Xu JW, Gong YX and Sun NL. A Review of Mechanical Characterization Techniques for Ultrathin Films Beyond Two-dimensional Materials. *Advanced Materials Science and Technology*, 2024;6(1):0632008. https://doi.org/10.37155/2717-526X-0601-5

Abstract: Thin films, thinner than the diameter of a human hair (~90μm and below), hold considerable promise across various applications such as flexible electronics, thin film devices, and biomedical applications due to their distinct characteristics. At this juncture, the mechanical properties of these films play a pivotal role as they underpin the stability of these applications. However, evaluating the mechanical properties of these thin films poses a significant technical challenge owing to their minimal thickness, where conventional technologies often prove inadequate. Over the past decade, notable advancements have been made in characterization techniques to surmount this challenge, particularly for ultra-thin films. This review focuses on recently developed

experimental techniques used for characterizing the mechanical properties of thin films thinner than the diameter of a human hair, but beyond two-dimensional materials. We introduce these experimental testing techniques, analyze their pros and cons, and discuss their main applications. The mechanical properties of ultrathin films beyond 2D materials discussed in this study include elastic modulus, hardness, in-plane strength, and fracture toughness. We conclude this review article with our perspective on the applications and future research directions of thin films in the current state of the field.

Keywords: Thin film; Mechanical property; Nanomechanics; Mechanical characterization

1. Introduction

The distinct characteristics and broad potential applications inherent in films thinner than the diameter of a human hair (~90 μm and below) have garnered significant attention. These thin films hold considerable promise across various domains, including but not limited to flexible transistors (TFTs)[1–3], characterization devices[4–6], biomedical electronics[7], and among others. For example, the exceptional thermal/electrical/optical properties of two-dimensional materials offer distinct advantages for its utilization in opto/electronics[8]; silicon nitride (SiN_x) thin films are widely used as encapsulation layer in many semiconductor devices, owing to their highly dense structure and inert characteristics[9]; organic thin films are also highly adopted to make flexible transistors with exceptional properties[3]; nanocomposite thin films were also developed that enabled in-chip resistive switching [5] and biocompatibility [7].

Notably, the mechanical attributes (e.g., elastic modulus, strength, and fracture toughness) of these films play a pivotal role, as they underpin the stability of the applications mentioned above, prompting extensive scrutiny[10,11]. Nevertheless, assessing mechanical properties in these delicate film structures presents a formidable technical hurdle due to their exceptionally diminutive thickness. Conventional mechanical testing methodologies often must be revised for materials at such minute scales. For instance, when the thickness of the film is significantly smaller than that of the substrate, distinguishing a minuscule force applied to the thin film from the comparatively substantial force acting on the film/substrate composite becomes challenging. Although basic solutions, like the 'rule of the tenth' for nanoindentation, may not cover all errors related to substrate effects in thin film measurements, significant progress has occurred in the past decade. Specialized experimental characterization techniques have emerged, directly tackling the challenges associated with ultrathin films. To circumvent the substrate effects in traditional tensile tests, Kim et al.[12] used the water surface as a suitable substrate for supporting free-standing ultra-thin films. They introduced a pseudo-free-standing tensile testing technique enabling nearly frictionless stretching without any substrate effects or specimen damage. Subsequently, other novel technologies or improved techniques were developed including mechanical testing of substrate-free or free-standing thin films[13–18]. These technologies achieved the goals of directly measuring the complete stress-strain behaviors of the ultra-thin films while capturing their failure response. These enhanced techniques not only mitigate the substrate effects but also expand the range of applicable thin films, such as metallic, organic, and hybrid materials, thereby providing new opportunities for the mechanical characterizations and the further applications of these thin films.

To accurately measure the mechanical properties of thinner films while overcoming the limitations of traditional techniques in future advancements, a retrospective analysis of the development trajectory of mechanical characterization techniques for thin films can provide valuable experiential insights. Therefore, this mini-review delves into recently developed experimental techniques for characterizing the mechanical properties of films thinner than the diameter of a human hair, extending beyond two-dimensional materials. This involves introducing experimental testing techniques, analyzing their pros and cons, and discussing their main applications. Notably, as there are numerous review articles available that extensively cover two-dimensional materials (i.e., films below 2 nm), they will not be included in this review, this paper only summarizes the research methods of thin films in the range of 2nm to 100 microns. The mechanical properties to be discussed in this review include elastic modulus,

hardness, in-plane strength, and fracture toughness.

2. Characterizations of mechanical properties

2.1 Elastic modulus and hardness

2.1.1 Nanoindentation

The nanoindentation technique is commonly used for measuring the elastic modulus (E) and the hardness (H) of thin films in this thickness range. Indentations are made on the material surface by a micro-indenter, and E and H can be calculated by fitting the captured load-displacement curves using contact mechanics models. The Oliver-Pharr's nanoindentation model has been predominantly used to measure the elastic modulus and hardness of thin films[19–29].

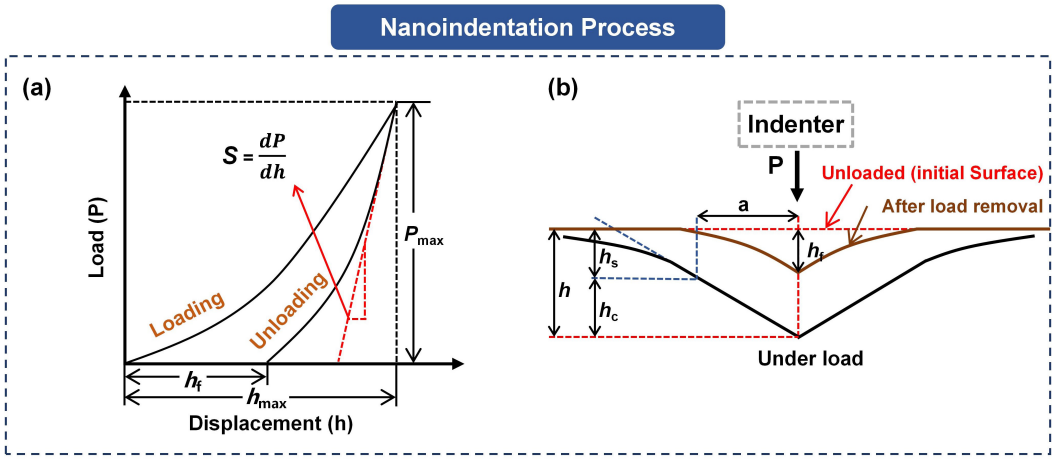

Figure 1. Representative schematic of the nanoindentation process. (a) Typical loading and unloading curves. The quantities shown are P_{max}: the peak indentation load; h_{max}: the indentation displacement at peak load; h_f: the final depth of the contact impression after unloading; and S: the initial unloading stiffness. Reproduce from [10]. (b) Schematic diagram of the loading process. The unloaded surface (red line), after-load removal surface (brown line), and the under-load surface (black line) show the deformation behavior of the sample. The quantities shown are P: the indentation load; h: the total indenter displacement; h_f: the final depth of the contact impression after unloading; h_s: the displacement of the surface at the perimeter of the contact; h_c: the vertical distance along which contact is made; and a: the radius of the contact area. Reproduce from [10].

This model provided an analytical solution to obtain the mechanical properties of thin films while considering the geometry of the indenters and their depth of the impression after the elastic unloading. From the indentation load-displacement data as shown in Figure 1a, the stiffness S can be experimentally measured to determine the reduced elastic modulus E_r from the following relation,

$$E_r = \frac{\sqrt{\pi}}{2}\frac{S}{\sqrt{A}}\# \quad (1)$$

where A is the projected area computed from h_c, the vertical distance along which the contact is made referring to Figure 1(b). Knowing the Young's Modulus of the indenter E_i, and its Poisson coefficient v_i, the Young's modulus of the thin film can be calculated using the equation,

$$\frac{1}{E_r} = \frac{\left(1-v^2\right)}{E} + \frac{\left(1-v_i^2\right)}{E_i}\# \quad (2)$$

As hardness is defined as the maximum indentation load the material would support, it can be obtained from

$$H = \frac{P_{max}}{A}\# \quad (3)$$

Characterizing ultrathin films by nanoindentation is challenging because substrate effects become prominent compared to thicker films tested under similar setups. Substrate effect refers to the influence of the underlying material or surface on the behavior or properties of a component or structure. In the presence of a substrate beneath a film, inappropriate indentation depth can cause the measured properties to be influenced by the substrate. This effect can be avoided by using the "rule of the tenth", which ensures that the indentation depth is less than 10% of the film thickness. The roughness of the film surface should also be considered to determine the appropriate indentation depth[18–20]. For example, Gao et al.[21] assumed that the SiC substrate

in their experiment did not influence the indentation test to disregard the substrate effect. This assumption was based on the shallow indentation depth of 0.1 nm and the graphene being ten layers thick with a total estimated thickness of 3 nm. However, minimizing the penetration depth of the probe into the sample to less than 10% of the total film thickness is suggested to mitigate the influence of the substrate effect, but it is not suitable for ultrathin films. Significant efforts have been devoted to incorporating substrate effects.

During the development of the contact mechanics model, three classical models (i.e., Hertz[22], Johnson-Kendall-Roberts (JKR)[23], and Derjaguin, Muller, and Toporov[24] (DMT) models are worth discussing. In 1882, Hertz[22] addressed the deformation of elastic spherical surfaces in contact under an applied load, assuming no adhesion between them. His model solved the contact between a hemisphere and a rigid plane. Based on Hertz's model, Johnson et al.[23] and Derjaguin et al.[24] derived JKR and DMT models, respectively, that take contact area into account. JKR model that utilizes data points on the unloading portions of the force-separation curve for elastic modulus calculation considering the surface energies of the contact surfaces. Then, the influence of the adhesive interaction between the probe and the sample can be quantified. Derjaguin et al.[24] proposed incorporating the energy of molecular attraction within the ring-shaped region of non-contact adhesion in addition to Hertz's model. The DMT model considers surface interactions and first determines the contact deformation and the molecular attraction of a ball to a plane. In comparison, Hertz's theory is only applicable when the adhesion force is significantly smaller than the maximum load. JKR model is well-suited for soft materials characterized by high surface energy and a substantial contact area. In contrast, the DMT theory applies more to scenarios involving small, rigid surfaces with low surface energy[25]. Butt et al.[26] summarized the relation between the contact radius a, sample deformation d, and the adhesion force F_{ad} for a spherical tip on a flat surface in Hertz, JKR, and DMT models.

Rather than the three models above, many other models use alternative methods to achieve more accurate measurements. Jönsson and Hogmark[26] introduced the correlation between the hardness of composites and intrinsic hardness. Knowing the film thickness, the composite hardness and the substrate hardness, the model enables the determination of characteristic hardness values for films with thicknesses as low as a few thousand angstroms, which applies to films that are harder than the substrate. Doerner et al.[27] proposed a model that rates an empirical function based on the contact depth to consider both the film and substrate contributions, which permits the detection of the influence of the substrate. However, the accuracy of Doerner's model diminishes as it is employed on thin films, significantly when the ratio of punch size to film thickness increases since the importance of the substrate material's elasticity increases. King[28] improved and expanded Doerner's model, making it applicable for flat-ended cylindrical, quadrilateral, and triangular indenters while increasing the accuracy of elastic modulus measurement. Furthermore, Saha and Nix[29] modified the analysis in King's method to calculate the elastic modulus of the tested thin film from the reduced elastic modulus data, assuming that the tip of the Berkovich indenter can be approximated as a flat punch. They introduced the effective film thickness to replace the apparent film thickness to decouple the combined response from the film and the substrate.

Some methods considering other factors (e.g., continuous stiffness measurement or CSM technique, discontinuity in elastic strain transfer) have also achieved significant results in addressing the substrate effect. Gao et al.[30] focused on the complete energy conversion process during indentation and derived the closed-form solution using the first-order perturbation theory. The solutions of this modulus perturbation model in their experiment enabled the estimation of the unloading compliance of the tested thin film during the test and could be extended to more complicated elastic contact problems for a nonhomogeneous material. Zhou et al.[31] utilized the CSM technique to obtain the original analysis data. The hardness of the film is calculated by plotting P/S^2, which is not dependent on the contact area, to avoid the effects of substrate contribution and material pile-up behavior. This approach provides a simple method for determining the actual hardness of soft metallic thin films. More recently, Zhou and Prorok[32] developed a novel model considering the presence of an apparent discontinuity in elastic strain transfer at the interface between the film and substrate. Provided that the bulk Poisson's ratio is known, their model could evaluate the elastic modulus

of thin films that do not display a flat region.

In the past five years, the nanoindentation technique has continued to be widely used for determining the elastic modulus and hardness of thin films. Ma et al.[33] performed indentation tests on Fe-O films with a thickness of 1.8 μm using reactive magnetron sputtering under different preparation conditions. They analyzed the effects of annealing temperature and oxygen injection flow rate on the mechanical properties of the films. Lekoui et al.[34] determined the mechanical properties of a series of TiAlN films with thicknesses ranging from 517 to 586 nm via CSM and the Oliver-Pharr method to investigate the impact of deposition time on the films' properties. Kim et al.[35] obtained the CSM data of Ni-Mo-W thin films with thicknesses ranging from 410 to 890 nm using Diamond Berkovich tips and successfully determined the Young's modulus and hardness of the tested films. Boughrara et al.[36] investigated the mechanical properties of $Al_xGa_{1-x}N$ films using an instrument equipped with a pyramid-shaped Berkovich-type diamond indenter and analyzed the results through the Oliver-Pharr model. Their findings revealed a strong dependency on the physical and nanomechanical properties depending on the degree of coalescence on the film surface. Manica et al.[37] performed nanoindentation on Al_2O_3 films fabricated by pulsed laser deposition (PLD). Their research demonstrated that the PLD technique enables the acquisition of Al_2O_3 coatings with mechanical properties comparable to those achieved through other deposition methods. Maruyama et al.[38] tested the Young's modulus for $BaTiO_3$ film samples at five different thicknesses ranging from 10 to 30 μm, through nanoindentation using a Bercovich indenter. The analyzed result based on the Oliver-Pharr model showed that the elastic modulus of the films increases from approximately 130 to 160 GPa with annealing. Dziri et al.[39] applied Jönsson and Hogmark's model to measure the hardness of Constantan thin film on silicon (Si) wafer. They discovered that the Constantan film's hardness was consistent, whereas the substrate's hardness changed with film thickness due to brittleness and cracking at the interface. Valour et al.[40] measured the hardness of the TiN film, which was produced by converting the TiO_2 film precursor through thermal nitridation in an ammonia atmosphere through Zhou's method. The hardness value and the measurement result of optical and electrical properties of TiN thin film suggested that TiN thin films produced via the sol-gel method and rapid thermal nitridation hold great potential for use in the fabrication of optical metasurface devices and novel plasmonic materials. Yang et al.[41] performed nanoindentation on amorphous carbon films prepared by magnetron sputtering deposition and successfully analyzed the effect of heat treatment on the material. For group III-V films, Yang et al.[42] obtained the Young's modulus and hardness of GaN thin films through nanoindentation using a three-sided pyramidal Berkovich diamond indenter via CSM technique, where it is worth noting that they controlled the indenter only 200 nm deeper to avoid substrate effects. Li et al.[43] evaluated the elastic modulus of $CaTiO_3$ dielectric thin films with thicknesses from 65 nm to 340 nm. In conjunction with the hardness measurement results, their research showed that it is possible to effectively adjust the mechanical properties through film thickness and grain size control. This may facilitate the development of high-performance microwave dielectric devices for future applications. R. Garcia[44] and J. Y. Park et al.[45] introduce state-of-the-art force microscope-based methods for mapping the elastic and viscoelastic properties of soft materials (including 2D atomic sheets, such as graphene, MoS_2, and boron nitrides) at high spatial resolution, it is elucidated that nanoindentation technique is a fast, high-resolution, non-destructive and quantitative characterization methods to develop materials with nanoscale customizable properties. A more detailed study is conducted by G. Cortelli et al.[46] to study the nanomechanics of ultrathin gold films on a PDMS elastomer using an analytic model describing the indentation for a discrete stiff layer on a compliant substrate[47].

2.1.2 Tensile test

The tensile test is also a common characterization technique for thin films to measure their global properties (i.e., elastic modulus, strength, and fracture toughness) in contrast to local properties characterized by the nanoindentation test. It quantifies the force necessary for the fracture of a composite or plastic sample and the degree to which the specimen experiences elongation or stretching before reaching the fracture point. Figure 2a shows a typical stress-strain curve from which the mechanical properties could be calculated[48]. A tensile test device is shown

in Figure 2b, where a multilayer film is mounted in a copper clip of two slides, and a force is applied to the film by a freely moving slider. A sensor records this process. The laser beam is directed towards the sample's surface and is subsequently diffracted by the grating. The measurement of tensile displacement in the film is accomplished by assessing the travel distance of the laser spot. Determination of stress is achieved by measuring the applied load and the sectional area, while the elastic modulus is derived from the slope of the unloading curve. In this experiment setup, Huang et al.[49] used typical tensile experiments to determine the elastic modulus of 59 groups of free-standing Ag/Cu multilayer films with a thickness of 3 nm to 3 μm. The accurate measurements mitigated the “supermodulus” effect that was previously reported.

Similarly, substrates can influence the measurement results in the tensile test. To minimize the effects caused by solid substrates, there has been a growing interest in using liquid-based substrates (e.g., water), then it came to film-on-water (FOW) tensile tests. Water exhibits high surface tension and low viscosity, offering a nearly frictionless sliding environment in tensile test[12]. In 2007, Huang et al.[50] discovered that a droplet of water placed on a floating polymer film resulted in distinct wrinkling patterns. This provides an opportunity for determining the relaxation properties, elastic modulus, and thickness of ultrathin films. In 2013, Kim et al.[12] proposed the pseudo-free-standing tensile test (PFSTT) technique where all tested thin films and the experiments are performed on either the surface of water or a water-diluted etchant solution for easy handling and almost frictionless sliding without any substrate effects or specimen damage. The specimen fabrication and transfer processes are shown in Figure 2c. A “dog-bone” specimen is produced, and then the specimen is transferred onto a water surface. The experiment diagram of the PFSTT technique is shown in Figure 2d, where a load cell, a linear stage, and a Digital Image Correlation (DIC) camera situated on an anti-vibration table are involved. The load cell is used to quantify the force. The high-resolution linear DC motor, along with a corresponding controller, is employed to achieve linear displacement. The DIC system is established by employing a charge-coupled device (CCD) camera with a microscope, enabling continuous real-time monitoring of the specimen's strain during the testing process. Micro XYZ positioning stages are positioned beneath the load cell and the linear stage to facilitate the precise alignment of the film. Kim et al. successfully applied tensile forces to the floating specimens and directly measured the stress-strain curves. Similar to the applications of PFSTT to polymer thin films, Liu et al.[13] introduced a new method called the ultra-thin film tensile (UFT) technique that can directly measure the complete stress-strain response of the ultra-thin films under uniaxial tension. As presented in Figure 2e, the setup incorporated a laser reflection from a displacing cantilever for force sensing and a linear actuator for displacement, allowing gentle and stable stretching and sensing at macroscopic level such as the characterization of the uniaxial stress-strain relationship within constrained molecular networks. Similarly, Bay et al.[14] proposed the Uniaxial Tensile Tester for Ultrathin Films (TUTTUT) technique. As indicated in Figure 2f-g, by laser-cutting the sample into a "dog-bone" configuration and the stress concentration was significantly reduced compared to the rectangular specimen. The integration of a dark field microscope objective into the experimental setup further allows for the direct measurement of the complete stress-strain relationship in the extension of ultrathin polymer films with real time imaging.

In 2019, Bay et al.[15] noticed that the measured mechanical properties of the tested polystyrene (PS) thin films also suffer from the influence of the support of liquid. They proposed the measurements of the uniaxial stress-strain response that can capture the failure response, referring as Tensile tester for Ultrathin Freestanding Films (TUFF) technique. Figure 3a-b shows lifting a polymer film from a water surface onto a support frame and a diagram of a "dog-bone" laser-cut freestanding film, respectively. In the TUFF setup as indicated in Figure 3c, a metal frame was used to overcome the capillary force of the water, the frame had a slotted opening and three edges allowing the free-standing thin film to hold after being picked up off the water surface. More recently, in 2021, Galuska et al.[16] proposed a robust transfer technique called Shear Motion-assisted Robust Transfer (SMART) technique for the fabrication of free-standing sub-100nm films and the measurement of their intrinsic mechanical properties. Compared to water-assist measurement, a shear motion removes the water bath from beneath the film, resulting in a free-

standing dog bone ready for tensile analysis as shown in Figure 3d. The SMART technique introduces a novel approach for investigating the mechanical properties of thin films and even 2D materials.

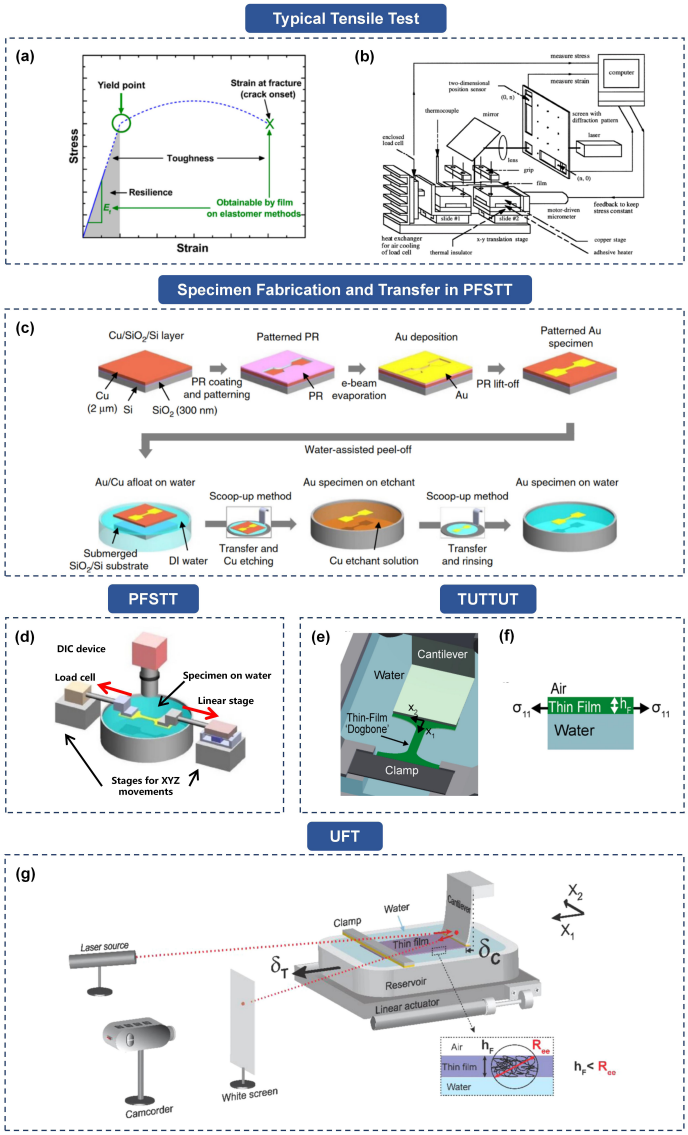

Figure 2. Representative equipment setup and specimen fabrication for typical tensile tests, PFSTT, UFT, TUTTUT, and TUFF techniques. (a) Hypothetical stress−strain curve showing the critical features[48]. Copyright (2015), American Chemical Society. (b) Schematic diagram of the micro-tensile test setup[49]. Copyright (2000), with permission from Elsevier. (c) Schematic diagram of the specimen fabrication and transfer processes in PFSTT technique[12]. The upper section outlines the process for producing a "dog-bone" Au thin film specimen. The lower section provides an overview of the procedures to transfer the Au specimen onto a deionized (DI) water surface, utilizing water-assisted mechanical peel-off and Cu wet etching. Reprinted by permission from Springer Nature Customer Service Centre GmbH: Springer Nature, Nat. Commun12© 2013. (d) Schematic diagram of PFSTT technique[12]. The equipment is comprised of a load cell, a linear stage, and a Digital Image Correlation (DIC) camera situated on an anti-vibration table. Reprinted by permission from Springer Nature Customer Service Centre GmbH: Springer Nature, Nat. Commun[12]. © 2013. (e) Schematic diagram of UFT technique[13]. h_F, the film thickness that can be effectively tested is approximately equivalent to Ree, the end-to-end distance of the polymer chain within the bulk material. δ_C is the deflection of the cantilever. δ_T is the total displacement. Copyright (2015), American Chemical Society. (f) Schematic diagram of TUTTUT technique14. Copyright (2018), American Chemical Society. (g) Schematic diagram of the side view of stretching a "dog-bone" film on the surface of water[14]. Copyright (2018), American Chemical Society.

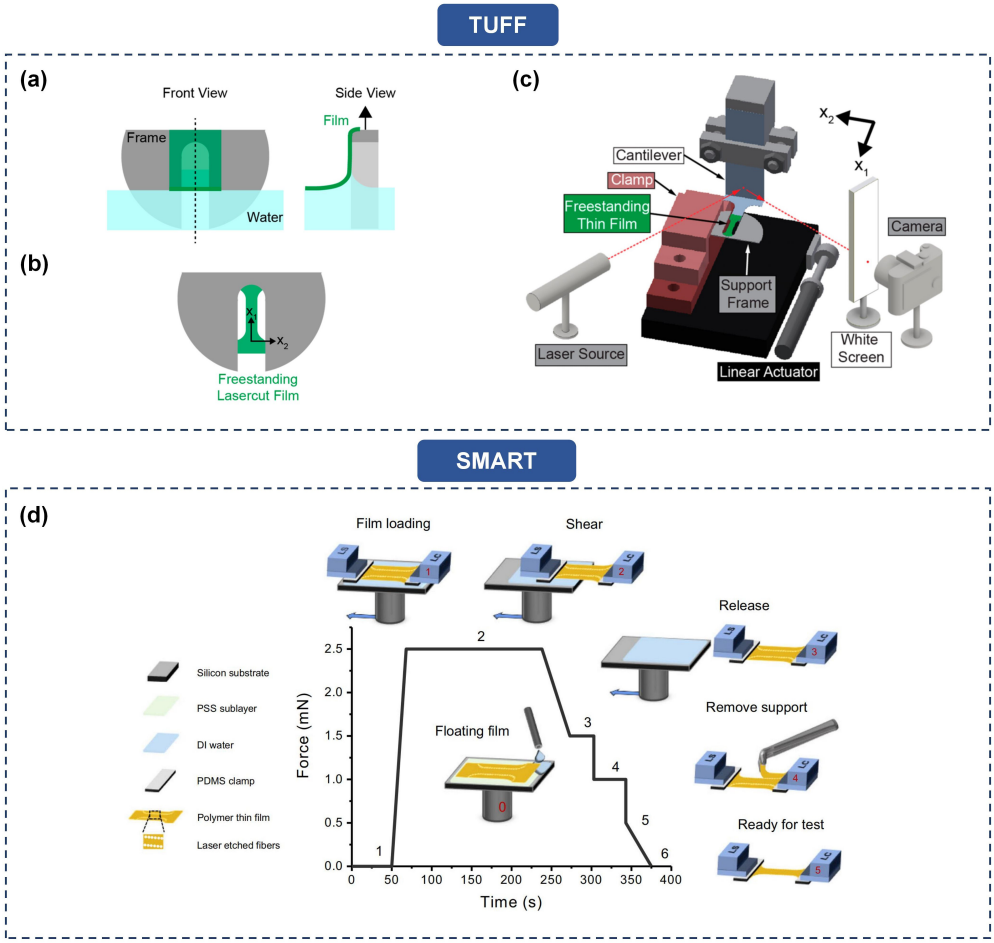

Figure 3. Representative equipment setup and specimen fabrication for TUFF and SMART techniques. (a) Schematic diagram of lifting a polymer film from a water surface onto a support frame[15]. The side view perspective is depicted from the dashed line. Copyright (2019), American Chemical Society. (b) Schematic diagram of a freestanding film with a "dog-bone" shape that has been laser-cut[15]. Copyright (2019), American Chemical Society. (c) Schematic diagram of TUFF experimental setup[15]. Copyright (2019), American Chemical Society. (d) Process diagram of SMART technique[16]. Removal of the water bath to obtain a free-standing film with a "dog bone" shape. Reprinted with permission from Springer Nature Customer Service Centre GmbH: Springer Nature, Nat. Commun[16]. © 2021.

Tensile tests are widely employed for the measurement of the elastic modulus of thin films. Particularly, FOW tensile tests are considered the appropriate and applicable approaches for polymer thin films. Kim et al.[12] applied the PFSTT technique to test the elastic modulus of Au thin films with thicknesses of 55, 85, and 400 nm on the $Cu/SiO_2/Si$ substrate. A decline in the elastic modulus decreased from 67 to 55 GPa as the thickness decreased from 400 to 55 nm. Likewise, Koo et al.[51] conducted the PFSTT technique to measure the elastic modulus of freestanding 100nm thick ALD Al_2O_3 thin film, where the findings suggest that higher elastic modulus values were achieved from the films produced at elevated deposition temperatures. Zhang, Song et al.[52] expanded the PFSTT technique to quantify the inherent mechanical properties of P3HT and a DPP-based polymer by conducting experiments under various conditions, including tests with different strain rates, stress relaxation, and hysteresis. Both P3HT and DPP-TVT exhibited an elevation in elastic modulus as the strain rate increased, reaching values of 135 to 360 MPa and 145 to 250 MPa, respectively. To determine the moduli of phase-separated thin films of polyurethane/polystyrene blends with thicknesses ranging from 135 to 675 nm, Zhang, Hong et al.[53] designed a double-sided adhesive frame as a replacement for the PDMS based on the PFSTT technique. The results showed that the deviation between the measured effective moduli

and the values calculated using existing models is attributed to the variations in phase height between the phase-separated domains, where the phase height difference is a topographical feature in blended thin films. Saito et al.[54] measured the elastic modulus of ultrathin polystyrene-b-polybutadiene-b-polystyrene (SBS) block copolymer (BCP) films with thicknesses from 20 to 600 nm using the PFSTT technique. The result showed that for SBS films thinner than 100 nm, the elastic modulus of the films increased significantly as the thickness decreased. In another experiment, Saito et al.[55] used the same method to study the elastic modulus of ultrathin polystyrene-b-polyisoprene-b-polystyrene (SIS) films containing 14 wt% PS with different thicknesses (30-1000nm) at different strain rates. The findings indicated a significant increase in elastic modulus as the film thickness decreases, even though only a limited number of PS-rich layers comprising dispersed cylindrical and spherical PS domains are present at the surface and interface. Kim et al.[56] employed the PFSTT technique to directly yield the elastic modulus of as-cast and annealed P(BDT2T): P(NDI2T) blend and PBDT2T-b-PNDI2T films. The annealed blended film exhibited an elastic modulus that closely approximates the elastic modulus observed in the as-cast blend film, while the crack-onset-strain (COS) and the fracture toughness of the annealed blend film increased. Oh et al.[57] investigated the intrinsic mechanical characteristics (i.e., elastic modulus, elongation, and fracture strength) of Plasma-enhanced chemical vapor deposition (PECVD) SiN_x thin films with thicknesses ranging from 130 to 150 nm through the PFSTT technique. The quantitatively determined intrinsic mechanical properties of SiNx thin films can be employed in mechanical analyses, including neutral axis analysis and finite element analysis (FEA), to predict failures.

Liu et al.[13] used the UFT technique to probe the stress-strain response of PS films with thicknesses ranging from 15 to 220 nm. The result showed a significant reduction in the elastic modulus, strain at failure, and nominal stress at failure for film thicknesses reaching as low as 15nm, providing novel perspectives on the changes in polymer chain entanglements within confined states. Bay et al.[14] used the TUTTUT technique to directly measure and observe the transitions in glassy polymer films controlled by thickness (20-360 nm). In alignment with the impact of surface mobility on strain localization, the elastic modulus of the films decreases at the thicknesses where shear deformation zones (SDZ) occur. Keren et al.[58] employed the TUTTUT technique to measure the mechanical properties of the SIS-based hybrid AlO_x-poly-(methylmethacrylate)(PMMA) thin films under an aqueous environment. Their findings showed that the elastic modulus and yield stress display an intricate, non-monotonic relationship with the increase in AlO_x volume fraction within PMMA upon contact with water. Some literature mainly probed other characteristics of thin films, reported the performance of thin films comprehensively, or designed some beneficial compound (e.g., Photocrosslinker), etc. They also measured the elastic modulus of the thin films[59–61], but elaboration on specific details for such experiments will not be included within this section. Bay et al.[15] tested the elastic modulus of ultra-thin freestanding PS films with thicknesses from 30 to 100 nm using the TUFF technique. Consistent elastic modulus and maximum stress were observed in the results even as the film thickness decreased to values as low as 30 nm. Galuska et al.[16] applied the SMART technique to measure the elastic modulus of PS thin films with thicknesses from 19 to 67 nm. Enhancement in strain at failure and a reduction in yield stress were observed. Notably, the modulus experiences a reduction only in the case of the thinnest 19 nm film.

2.1.3 Bulge test

In 1959, Beams et al. pioneered bulge testing for thin films to assess their in-plane mechanical characteristics[62]. Unlike traditional nanoindentation or micro-tensile tests, bulge tests enable precise evaluate thin film properties without substrate effects but require some sample preparation such as lithography and etching techniques to prepare free-standing films[63]. The test involves measuring the relationship between applied pressure and resulting bulge deflection as indicated in Figure 4a, offering valuable insights into the thin film's mechanical properties, more specifically the elastic modulus. To perform the test, the thin film is deposited on a specially designed apparatus as shown in Figure 4b, featuring a rigid frame with a central aperture for controlled pressurization. A pressure differential is created by introducing pressurized fluid

into the cavity underneath the film, causing it to deform and create a bulge. Techniques such as scanning white light interferometer (SWLI), laser autofocus displacement sensor, and Michelson interferometer are employed to measure pressure-deflection behavior. Originally, bulging tests were used to measure the mechanical properties of circular thin films. Based on the shape of the tested thin film, bulging tests can be divided into three categories: circular, rectangular, and square. The widely preferred plane-strain bulge test effectively assesses the mechanical properties of thin rectangular films. For rectangular membranes with aspect ratios greater than 4, the center's deflection remains nearly independent of the aspect ratio, closely approximating plane strain during deformation[63]. In this case, stress and strain uniformly distribute across the thin films, enabling the study of both elastic and plastic behaviors. In such setup, the applied pressure on the film could be expressed as a function of the thin film's deflection h, elastic modulus E, Poisson ratio v, thickness of the thin film t, width $2a$, length $2b$, and its residual stress σ_0[64,65].

$$p(h) = C_1 \frac{\sigma_0 t}{a^2} h + C_2 \frac{Et}{(1-v)a^4} h^3 \# \quad (4)$$

where C_1 and C_2 are the geometry factors depending on the Poisson's ratio and aspect ratio b/a of the film[66,67]. For rectangular specimens with aspect ratios greater than 4, their length can be approximated as infinitely. Then, the above equation can be rewritten as[64]

$$p = 2\frac{\sigma_0}{a^2} \mathrm{h} + \frac{4}{3}\frac{E\mathrm{t}}{(1-v^2)a^4} h^3 \# \quad (5)$$

When the deflection h is much smaller than the membrane width $2a$, the stress σ and strain ε in the center of the tested film are[64]

$$\sigma = \frac{pa^2}{2ht} \# \quad (6)$$

$$\varepsilon = \frac{2h^2}{3a^2} + \varepsilon_0 \# \quad (7)$$

where ε_0 the residual plane strain. The elastic modulus E, and the residual stress σ_0, were extracted from the pressure-displacement curve by fitting an analytical expression for the pressure P as a function of the membrane deflection h.

The bulge test is widely used to determine the elastic modulus of the tested thin film, where the shape of the measured film can be rectangular, square, or circular. Rontu et al.[68] conducted the bulge test to determine the elastic modulus of freestanding ALD Al_2O_3 thin films with two different thicknesses (14.8 and 48.1 nm). The results showed a discernible increase in the elastic modulus for the thinner film, though the elastic modulus of 48.1nm was relatively low. Mongkolsuttirat et al.[69] studied the impact of solid solution (V) and oxide dispersion (V_2O_5) alloying on the viscoelastic relaxation properties of 500 nm thick Au alloy films through the bulge test within the temperature ranging from 20 to 80°C. The results showed that within the temperature range, incorporating V and V_2O_5 into Au thin films resulted in a substantial reduction in both the magnitude and the rate of viscoelastic and anelastic modulus decay compared to pure Au. Tinoco et al.[70] determined the elastic properties of freestanding thin Si_3N_4 films with thicknesses of 100 and 500 nm based on the bulge test and a numerical approach including classical analytical methods and FEA. The numerical results showed an agreement between the calculated load-deflection curves and the experimental measurements for thin square and rectangular films. Österlund et al.[71] applied the bulge test to determine the elastic modulus of aluminum nitride (AlN) thin films with thicknesses ranging from ~54.9 nm to ~220 nm, and the tested films were prepared by different deposition methods, including sputtering, metalorganic vapor phase epitaxy (MOVPE), and ALD. The deposition methods and the conditions can influence the microstructure, and the results showed that the film's microstructure mainly governs the elastic modulus of AlN. Notably, a microstructure characterized by a greater degree of crystallinity exhibits a higher elastic modulus. Recently, Montinaro et al.[72] proposed a novel experimental-numerical methodology that integrates experimental measurements with numerical simulations to assess the elastic properties of Al-coated PI thin films with thicknesses ranging from 45 to 450 nm. The key innovation in the approach involved using the initial height as a simulation parameter to align with experimental data. This addresses the challenge of accurately measuring the initial deflection of ultra-thin films (thickness < 100 nm) in the plane-strain bulge test, where slight pressure fluctuations can significantly impact results. The results finally demonstrated an excellent alignment between the experimental and simulated bulged profile across all the examined

geometries, affirming the reliability of the new approach.

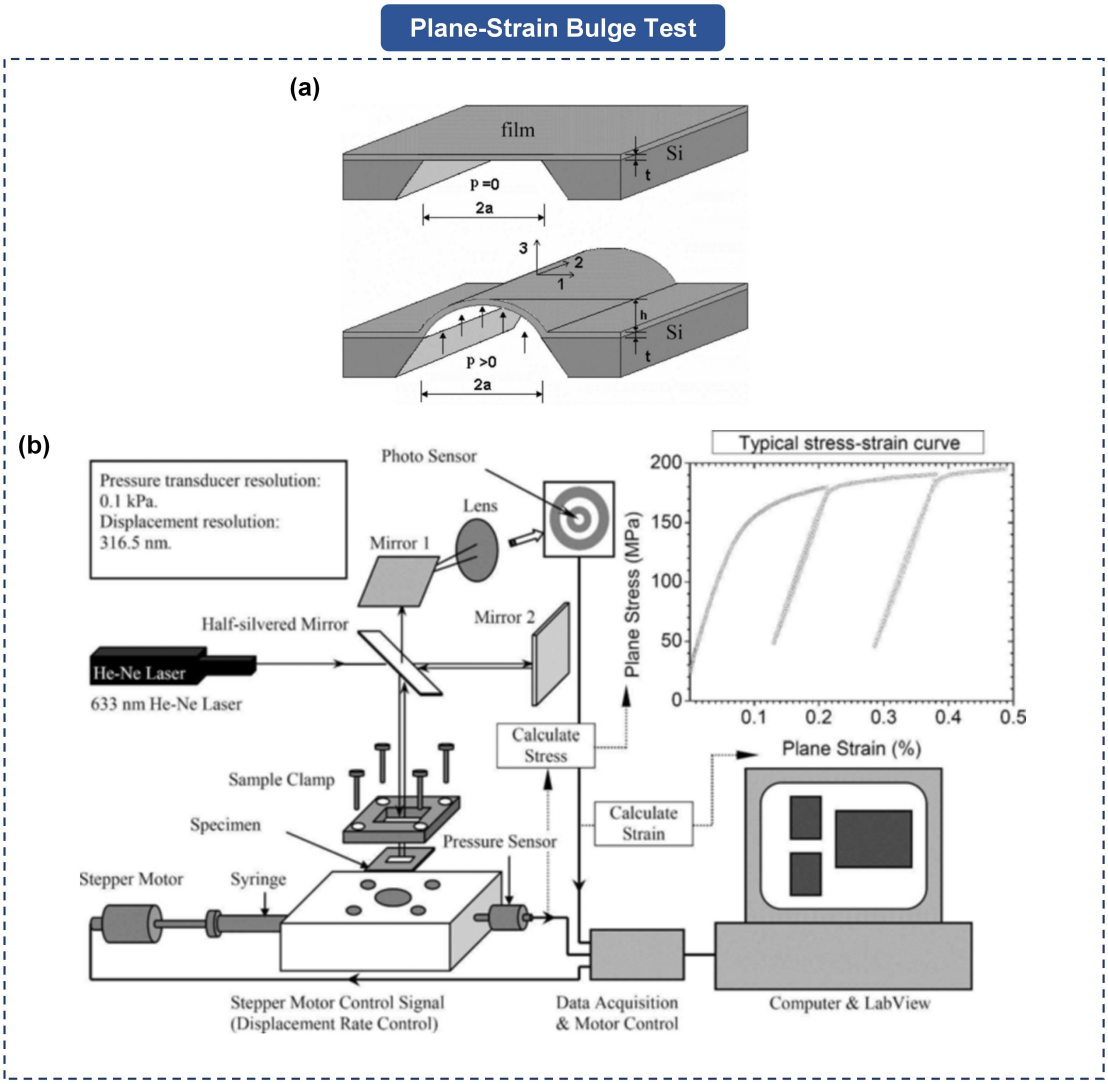

Figure 4. Representative schematic bulge test process. (a) Schematic diagram of the plane-strain bulge test before and after applying the load. Reprinted with permission from Springer Nature Customer Service Centre GmbH: Springer Nature, J. Mater. Res.[63] © 2005. (b) Schematic diagram of the bulge test apparatus. Reprinted with permission from Springer Nature Customer Service Centre GmbH: Springer Nature, J. Mater. Res.[63] © 2005.

2.1.4 Buckling-based test

To overcome the limitations of adaptability and combinatorial measurement in traditional methods, Stafford et al. introduced a rapid and cost-efficient method to characterize the mechanical properties of thin films down to nanoscale[73]. The SIEBIMM (strain-induced elastic buckling instability for mechanical measurements) is designed for measuring the elastic modulus of stiff film coatings on relatively softer substrate, utilizing the instability in bilayer structures. Illustrated in Figure 5a-c, the thin film on the specimen buckles under compressive strain due to substrate-film stiffness mismatch. The buckling instability exhibits a sinusoidal waveform with a critical wavelength (d) minimizing total strain energy, which depends on material properties. Solving for the elastic modulus of the upper film involves utilizing this critical wavelength in the following equation[73]:

$$\frac{E_f}{\left(1-v_f^2\right)} = \frac{3E_s}{\left(1-v_s^2\right)}\left(\frac{d}{2\pi h}\right)^3 \# \quad (8)$$

where E_f and v_f are the elastic modulus and Poisson's ratio of the film, E_s and v_s is the elastic modulus and

Poisson's ratio of the substrate, and h is the thickness of the upper film. Various techniques, including laser diffraction or atomic force microscopy, can be employed to assess the critical wavelength of the buckling instability. The conditions for applying the formula are as follows: (a) low strain ($\varepsilon << 10\%$), (b) $E_f/E_s >> 1$, (c) the substrate is much thicker than the membrane, and (d) the amplitude of buckling is much smaller than its wavelength[73,74].

In 2018, Rencheck et al.[75] identified some other limitations in the SIEBIMM technique: (1) Surface wrinkles are unsuitable for characterizing films with thicknesses surpassing 1 μm. (2) There is a need for specific interfacial interactions between the two materials for the film to be adequately adhered to the substrate. (3) Sample preparation is more intricate than more straightforward methods, as the SIEBIMM technique necessitates floating and attaching thin films onto soft substrates. To address these issues, a free-standing column buckling (FSCB) technique was innovated to facilitate the measurement of the elastic modulus of glassy polymer films[75]. The equipment to perform FSCB test consisted of a miniature load cell, a fiber optic displacement sensor, and two linear piezo motorized stages, as illustrated in **Figure 5f-g**. thin film specimen was attached to the center of sample holders using cyanoacrylate glue, which was applied to the sample's center and spread evenly across the sample holder using a cotton swab, creating a liquid glue layer. During each test, a compressive axial load is applied to a glassy thin film at a constant displacement rate until an out-of-plane buckling instability is induced. Figure 5d provides a schematic depiction of a free-standing column before and after buckling, and a representative load-displacement result for a typical buckling-based metrology is shown in Figure 5e. Figure 5h-k shows the oblique and top-down views of the film before and after the load reaches P_{cr}. The elastic modulus E of the elastically buckled column is calculated by.

$$E = \left(\frac{3}{\pi^2}\right) P_{cr} \left(\frac{a^2}{bh^3}\right) \# \quad (9)$$

where P_{cr} is the critical buckling load, a is the length of the thin film and b is the width of the thin film.

Buckling of the film through mechanical compression or thermal shrinkage has been extended to measure the elastic modulus in a variety of thin films. Although the SIEBIMM technique is highly suitable under low strain, Li et al.[76] used this method to investigate the elastic modulus of 150 nm thick nanoporous gold (NPG) films under high strain creating wrinkles using heat-shrinkable substrates. The results indicated that the SIEBIMM technique was well adopted, where the calculated elastic modulus and the experimentally measured value are close to the value found in the literature. In the field of polymer film research, the buckling-based method is employed widely. Stimpson et al.[77] employed both uniaxial and biaxial thermal shrinking techniques alongside the mechanical compression SIEBIMM technique on cellulose nanocrystals (CNC) and polyethyleneimine (PEI) layer-by-layer films with thicknesses from tens to hundreds of nanometers. Comparing the results from three different methods, Stimpson et al. suggested biaxial thermal shrinking for high-throughput mechanical characterization of thin-film due to its high precision, low sensitivity, and simple experimental setup. Though the SIEBIMM technique exhibits the lowest precision, necessitates the most extensive equipment, and is highly susceptible to minor fluctuations in measured variables among the three methods, it enables reversible deformation of samples, accommodating thermally sensitive materials without requiring heating, and can measure the impact of relative humidity (RH) on the mechanical properties of films. Niinivaara et al.[78] investigated the adaptability of SIEBIMM to assess the elastic modulus of polyvinyl alcohol (PVOH) coatings with various thicknesses (67 nm to 40 μm) on polydimethylsiloxane (PDMS) substrates. It was postulated that the applicability of the conditions in SIEBIMM might be constrained by the reduced wavelength homogeneity in thicker buckled coatings, although buckling does not exhibit an inherent upper thickness limit. Finally, the results validated that the elastic modulus could be measured for PVOH coatings up to a thickness of 35 μm. Rencheck et al.[79] used the FSCB technique to determine the elastic modulus of glassy polymer films. Compared to results obtained through tensile testing, modulus values ascertained via either buckling-based approach exhibited higher reproducibility, particularly for the geometrically thickest films that are frequently the most challenging materials to characterize under tension. The elaboration of some other literature not mainly focusing on the mechanical properties of thin films is also not included within this section[80].

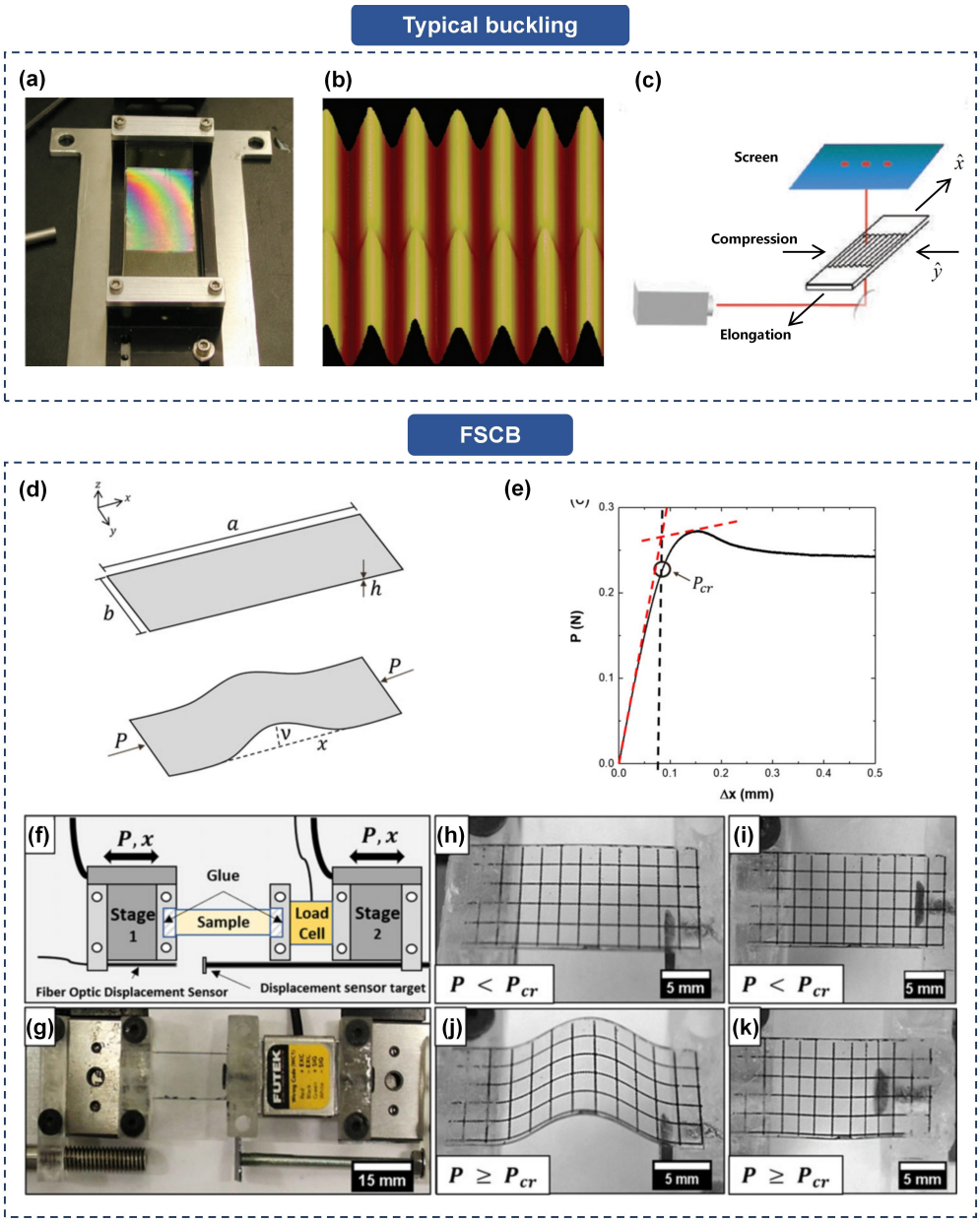

Figure 5. Representative equipment and example for buckling-based test and the FSCB technique. (a) A typical buckling-based test setup. Reprinted by permission from Springer Nature Customer Service Centre GmbH: Springer Nature, Nat. Mater[73]. © 2004. (b) The Atomic Force Microscopy (AFM) image illustrating the consistent sinusoidal buckling of the film in response to the compressive stress (with 0.3 μm amplitude and 8 μm wavelength). Reprinted by permission from Springer Nature Customer Service Centre GmbH: Springer Nature, Nat. Mater[73]. © 2004. (c) Schematic diagram of the custom-built small-angle light scattering of a low-power HeNe laser apparatus. The wavelength of the buckling is ascertained by measuring the dominant wavenumber. Reproduced by permission from Springer Nature Customer Service Centre GmbH: Springer Nature, Nat. Mater[73]. © 2004. (d) Schematic diagram of an unbuckled and a buckled film[75]. John Wiley & Sons. (e) Typical load (P)-displacement (Δx) curve in buckling experiment. The red dashed line and the black dashed line illustrate the tangent intersection approach and the displacement at which the thin film buckled, respectively. The value of the load at the intersection point of the black dashed line and the load-displacement curve represents the critical buckling load (P_{cr}).[75] John Wiley & Sons. (f) Schematic diagram of the experiment in FSCB.[75] John Wiley & Sons. (g) Top-down view of the experimental setup in FSCB[75]. John Wiley & Sons. (h, i) Oblique and top-down view of the film before the load reaches P_{cr}[75]. John Wiley & Sons. (j, k) Oblique and top-down view of the film after the load reaches P_{cr}[75]. John Wiley & Sons.

2.2 Strength

2.2.1 Tensile test

We mainly discuss the measurement of the yield strength and fracture strength in the 2.2 Section. The yield strength of the tested thin films is measured at the stress level when the transition from an elastic to a plastic deformation state occurs. In the standard tensile test, the yield strength of the ductile thin films is usually defined through the offset method[81], as shown in Figure 6a where a line is drawn parallel to the linear elastic region of the stress-strain curve with a 0.2% strain offset. The intersection of this offset line with the stress-strain curve gives the yield strength. The ultimate tensile strength can be measured at the highest point of the stress-strain curve.

The fracture strength of the tested thin films is characterized by the maximum stress at which the tested thin film experiences failure. The linear correlation between load and displacement comes to an abrupt cessation upon the initiation of specimen cracking, and then this discontinuity in the load-displacement curve enables the measurement of the critical load at the peak of the loading segment. Subsequently, the fracture strength is computed based on the critical load value. For brittle materials, due to the presence of a random arrangement of structural defections of varying sizes within them, their fracture strength exhibits a substantial degree of variability. The fracture strength decreases as the size of the defect increases. Then, generally, the measured strength of brittle materials is described by a Weibull model to extract the performance data[82], facilitating the examination of strength values by assessing failure probability at a specific stress level. The probability of failure P_f is expressed as

$$P_f = 1 - \exp\left[-\int_V \left(\frac{\sigma}{\sigma_0}\right)^m dV\right]\# \tag{10}$$

where m is the shape parameter known as Weibull modulus, σ_0 is the scale parameter known as characteristic strength, and V is the volume of the specimen. When the loading geometry is fixed, P_f can be expresses as

$$P_f = 1 - \exp\left(-\frac{\sigma_{max}}{\sigma_\theta}\right)^m \# \tag{11}$$

where σ_{max} is the maximum tensile stress and the σ_θ is the characteristic strength corresponding to a probability of failure of 63.2%. σ_θ can be calculated by[83]

$$\sigma_\theta = \sigma_0 V_{eff}^{-\frac{1}{m}} \# \tag{12}$$

where V_{eff}, the effective volume, can be calculated by[83]

$$V_{eff} = \int_V \left(\frac{\sigma}{\sigma_{max}}\right)^m \# \tag{13}$$

The maximum-likelihood estimation method is employed to calculate both σ_0 and m. A representative Weibull probability plot is shown in **Figure 6b**.

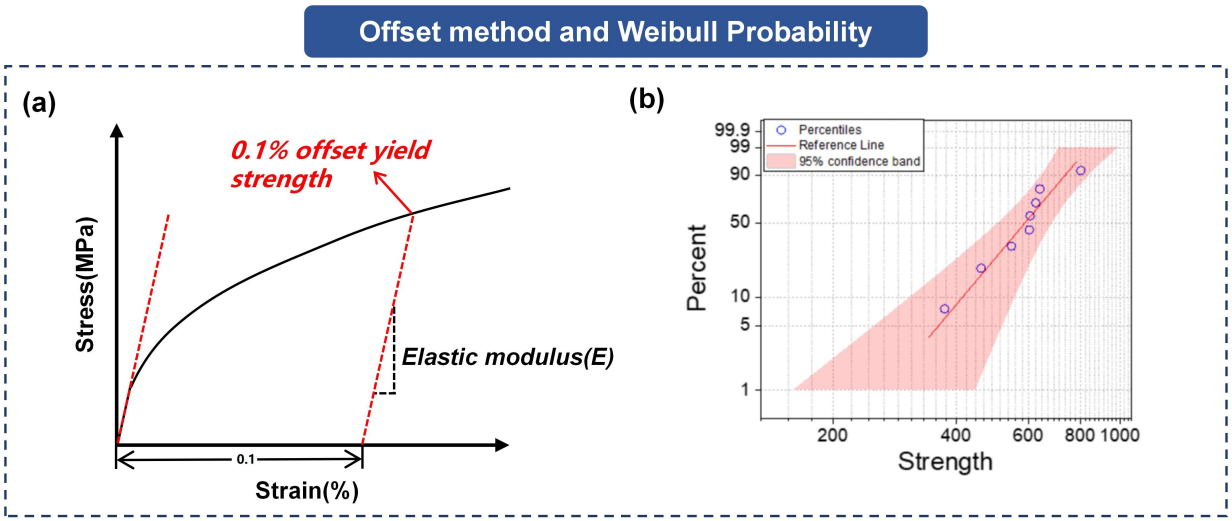

Figure 6. Representative schematic offset method in stress-strain curve and Weibull probability plot. (a) Stress-strain curve with 0.1% offset method. (b) Weibull probability plot of the strength for ALD Al_2O_3 films deposited at 200℃[51]. Copyright (2012), with permission from Elsevier.

Li et al.[84] analyzed and quantified the in-plane fracture characteristics of multilayer graphene nanosheets with thicknesses ranging from ~10 to 300 nm through in situ scanning electron microscope (SEM) and transmission microscope (TEM) tensile tests with Hysitron Push-to-Pull (PTP) micromechanical test devices. The results show that the fracture strengths of the nanosheets decrease with increasing thickness, attributed to defects and the presence of fracture layers, which follow a power law trend, but thinner nanosheets exhibit lower fracture strain values compared to their thicker counterparts. Jen et al.[85] conducted a study to obtain the yield stress and strain, and ultimate stress and strain of the 13 μm thick PE thin films to observe the formation of wrinkles for the original films using a micro tensile tester. Notched thin films with different holes (a central hole, two vertical holes, and two horizontal holes) are tested, and the strain-controlled mode is employed for the original films to conduct cyclic tension-tension (T-T) tests to obtain the strain-life curve. An instantaneous growth of the wrinkles was observed following the application of a load, and all three notched films were observed to have different generations of wrinkles. Min et al.[86] conducted the tensile test to assess the impact of the manufacturing technique on the mechanical properties of 12 μm thick copper thin films. The yield stress of 0.2% offset and the ultimate tensile strength of the rolled copper and the electrodeposited copper thin film were obtained. The results showed higher values for yield and ultimate tensile strength in the rolling process, revealing that copper thin films produced through the rolling process exhibit greater brittleness compared to those manufactured via the electrodeposition process. Berlia et al.[87] conducted the uniaxial tensile deformation experiment on freestanding Cu-Co nanolaminates with four different layer thicknesses (2, 4, 8, and 16 nm). Owing to the challenges associated with conducting uniaxial tensile tests at the micro/nanoscale, coupled with the time-consuming sample preparation procedures, the experiment was achieved using a specially designed microelectromechanical systems (MEMS) testing stage to evaluate the mechanical characteristics. A yield strength peak at a thickness of 4 nm was observed. Koo et al.[51] conducted the PFSTT technique to determine the strength of 100 nm thick freestanding ALD Al_2O_3 thin films produced at varying deposition temperatures. The results indicated that thin films fabricated at elevated deposition temperatures yielded higher values for strength, where the enhancement in strength was attributed to the diminishing hydroxide content that correlated with the escalation of the deposition temperature.

2.2.2 Bulge test

Similar to the measurement of strength in the tensile test, the yield strength, ultimate strength of thin films can be determined through the stress-strain curve in the bulge test. For the determination of the fracture strength, when considering the effect of residual stress, the fracture strength σ_f at the fracture pressure P_{max} in the bulge test can be determined by[68]

$$\sigma_f^3 - \sigma_0\sigma_f^2 - \frac{1}{24}\frac{E\left(P_{max}a^2\right)}{\left(1-v\right)t^2}\# \qquad (14)$$

By utilizing the previously determined residual stress and elastic modulus obtained from pressure-deflection measurements, it becomes feasible to calculate the fracture strength of the samples from the fracture pressures, which is achieved by finding the real root of Eq. 14.

Javed et al.[88] measured the yield strength of three SiNx-encapsulated metallic (Ag, Ti, and nickel-chromium alloy (NiCr)) thin films with 20 nm thickness. The NiCr thin films exhibited a yield strength that was one order of magnitude greater than that of Ag, whereas Ti demonstrated an intermediate level of yield strength. Tinoco et al.[89] measured the yield stress of a 1.74 μm thick freestanding thin Al film and identified the plasticity effect and the pressure inducing the transition from elastic to plastic behavior form the cyclic load-deflection data. The results observed plasticity effects commencing from the third loading cycle, and the plastic behavior of the film initiated at a stress level corresponding to the yield stress under biaxial tensile loading conditions. Gusev et al.[90] determined the maximum mechanical stresses of silicon oxide (SiO_2) thin films with thicknesses ranging from 226 to 2017 nm, deposited by plasma-enhanced chemical vapor deposition (PECVD). As the number of layers increases, a redistribution of mechanical stresses takes place. The layer-by-layer deposition of the films using the PECVD method can reduce the mechanical stress level, and a peak region is observed in the case of the four-layer film. Subjecting the films to heat

treatment resulted in a reduction of the relative error in estimating the mechanical strength value by more than two times. Rontu et al.[68] measured the fracture strength of freestanding ALD Al_2O_3 thin films with two different thicknesses (14.8 and 48.1 nm) using Eq. 14. It has been observed that the fracture strength of Al_2O_3 thin films exhibited a positive strain-rate dependency. Österlund et al.[71] determined the fracture strength of AlN thin films with thicknesses ranging from ~54.9 to ~220 nm prepared by different deposition methods using Eq. 18. The findings indicated that the fracture strength of AlN films was contingent upon the microstructural attributes of the film, influenced by the deposition methods employed. Films subjected to deposition at elevated temperatures exhibit superior crystal quality and subsequently demonstrate heightened mechanical robustness.

2.3 Fracture toughness

2.3.1 Nanoindentation test

The nanoindentation technique has gained growing prominence in measuring the fracture toughness of thin films due to its straightforward implementation. As shown in Figure 7a, a diversity of cracks may be generated in the surface of a brittle material by indentation contact. The classic indentation fracture mechanics model proposed by Lawn, Evans and Marshall (LEM model) examined the well-developed half-penny crack. Referring to Figure 7c, when the crack length c is larger than the contact size a, the LEM approach gives the expression of the fracture toughness K_C of a brittle material based on the hardness H and the elastic modulus E

$$K_C = \alpha\left(\frac{E}{H}\right)^{\frac{1}{2}}\left(\frac{P_{max}}{c^{\frac{3}{2}}}\right)\# \qquad (15)$$

where α is a constant depending on the geometry of the indenter, and P_{max} is the maximum pressure.

However, conventional approaches to fracture toughness measurement, which rely on a sharp indenter to induce radial cracking, become inapplicable as the cracking threshold often correspond to an indentation depth surpassing 10% of the thickness of thin films and the substrate effects is involved[91]. Instead, Li et al. developed a method to measure fracture toughness at low loads, identifying through-thickness cracking in the film from the analysis of load-displacement curves. The calculation of energy released during this cracking serves as a metric for fracture toughness. Three various stages in nanoindentation fracture are described in Figure 7b. In the first stage, the sharp indenter with a significantly small contact area can lead to the generation of high stresses within the contact region, particularly tensile stresses at the edges of the contact. In the second stage, the primary mechanism of the fracture of thin films during nanoindentation is attributed to the lateral expansion of volume and the presence of residual compressive stresses within the material beneath the indenter. In the third stage, the fracture mechanism of the thin film during nanoindentation is primarily governed by the significant bending stress exerted at the edge of the buckled film. Once the height reaches a critical value, the bending stresses induced by the bulged film around the indenter lead to the ring-like through-thickness crack formation of the film and subsequent spalling at the edge of the buckled film. Relating the work dissipated during film breaking with the "pop-in" phenomenon in the load-depth curve. The fracture toughness of the film can be written as

$$K_C = \left[\left(\frac{E}{\left(1-\nu^2\right)2\pi C_R}\right)\left(\frac{U}{t}\right)\right]^{\frac{1}{2}}\# \qquad (16)$$

where $A = 2\pi C_R t$ is the crack area, $2\pi C_R$ is the in-plane crack length of the coating, C_R is the radius of the circumferential thick-penetration crack formed around the indenter, U is the energy dissipated when the coating cracks, t is the effective thickness of the film, E and ν are the elastic modulus and Poisson's ratio of the coating respectively. Later, Toonder et al.[92] updated Li's method including the effective coating thickness and the count of cracks.

Energy-based approaches widely analyze thin film fracture toughness, accounting for the absence of elastic-plastic response changes in the coated system following Li's fracture method. Chen et al.[93] introduced the total work versus displacement curve to evaluate extremely small cracks within a thin film. This method can also differentiate the energy contributions from various deformation mechanisms apart from the energy dissipated during the fracture. A schematic plot of the total work-displacement curve is shown in Figure 7d. From the work-displacement curve, point A

is extrapolated to C, and point D is extrapolated back to point C to determine the total work dissipated in the fracture. AB denotes the work difference caused by different elastic-plastic deformation before and after the fracture. CD indicates the total work of the elastic-plastic deformation and fracture at the end of the cracking. The total work dissipated is obtained by CD minus AB. The value of the energy dissipated when the coating cracks is substituted by the estimated work to compute the fracture toughness. Similarly, Malzbender et al.[94] introduced an alternative energy-based model where the loading and unloading curves are integrated to determine the irreversibly dissipated energy during the indentation process. This information is then used to calculate energy release rates, enabling the derivation of fracture toughness. But interfacial damage, such as delimitation of the film around the indenter could affect the accuracy of the calculated the dissipated energy[95]. In cases the load-displacement curve does not have obvious slope change or discontinuity due to fracture, Chen et al.[96] proposed calculating the fracture dissipated energy and then the toughness from the total work of the indentation. The total work W_t is considered the sum of the work of plastic deformation W_P, the work of elastic deformation W_e, the fracture dissipated energy U_{fra}, and the other work W_{other}. With a specified indentation procedure, it is straightforward to measure both W_t and W_e. Assuming that the impact of a crack on the elastic-plastic deformation can be considered as an average effect across the entire loading curve, W_P can be approximated. The uncoated substrate was analyzed to obtain W_{other}.

In the past five years, the LEM approach and the energy-based approach have consistently been employed for measuring the fracture toughness of thin films. Cheng et al.[97] analyzed the effect of N_2/Ar flow ratios on the fracture toughness of ZrO_xN_y/V_2O_3 nano-multilayered films fabricated by magnetron sputtering with thicknesses ranging from 895 to 1306 nm. As the N_2/Ar flow ratios increase, the LEM approach calculated fracture toughness values of the films exhibited an initial increase followed by a subsequent decrease. The optimum fracture toughness value was measured at 0.879 MPa•$m^{1/2}$, indicating relatively good toughness. Soler et al.[98] applied the LEM approach to measure the fracture toughness of Mo_2BC thin films on Si (100) wafers with different substrate temperatures. Film thicknesses yielded ~3.82, ~3.75, ~3.77, and ~3.69 µm at temperatures of 380, 480, 580, and 630°C. It was observed that the fracture toughness exhibited a substantial decrease as the substrate temperature increased. Also, the decrease in the fracture toughness is accompanied by a consistent reduction in data scatter, attributed to the dependency of fracture toughness on the length of the crack. Pradeepkumar et al.[99] applied the LEM method and energy-based method to investigate the nano-scale load dependency of fracture toughness of indium tin oxide (ITO) coating (~1200 nm) on Si substrate. The results showed that the fracture toughness exhibited significant sensitivity to fluctuations in the applied load, and the energy-based method yielded higher fracture toughness. Jiang et al.[100] measured the fracture toughness of TiAlN thin films (1.4~2µm thick) deposited on Si(100) and AISI 304 austenitic stainless steel substrates by the deep oscillation magnetron sputtering (DOMS) using Li's method. The power applied to the sputtering process increased from 58.7 to 129.9kW, and the structure of TiAlN thin films was characterized by a face-centered cubic, and their composition was $Ti_{0.22}Al_{0.28}N_{0.50}$. Enhanced fracture toughness values of $Ti_{0.22}Al_{0.28}N_{0.50}$ thin films within Zone T were attained under a sputtering power of 90.2kW in the experiment. Wang et al.[101] investigated the impact of the layer structure on hysteresis behavior and cyclic deformation response of ITO/Ag/ITO (IAI) multilayer films with 180 nm nominal thickness, and the fracture toughness of the films was measured by energy-based method. A comparative analysis of the fracture behavior is conducted between fully annealed IAI multilayer films and ITO single-layer films, and the results showed that the fracture toughness of 300°C-IAI multilayer films exceeds that of ITO single-layer films, indicating a trend that aligned with the density of micro-cracks. Behboud et al. examined the mechanical properties of Zr_xTa_{1-x} thin films with x varying from 21% to 79% in atomic percent and ZrTa nanolayered films. Each film had a minimum thickness of 1 µm, and the fracture toughness was calculated using Chen's energy-based method. The 10 nm thick $Zr_{35}Ta_{65}/Zr_{70}Ta_{30}$ nanolayered film finally yielded a well-balanced combination of high fracture toughness, high strength, and a high density of shear banding.

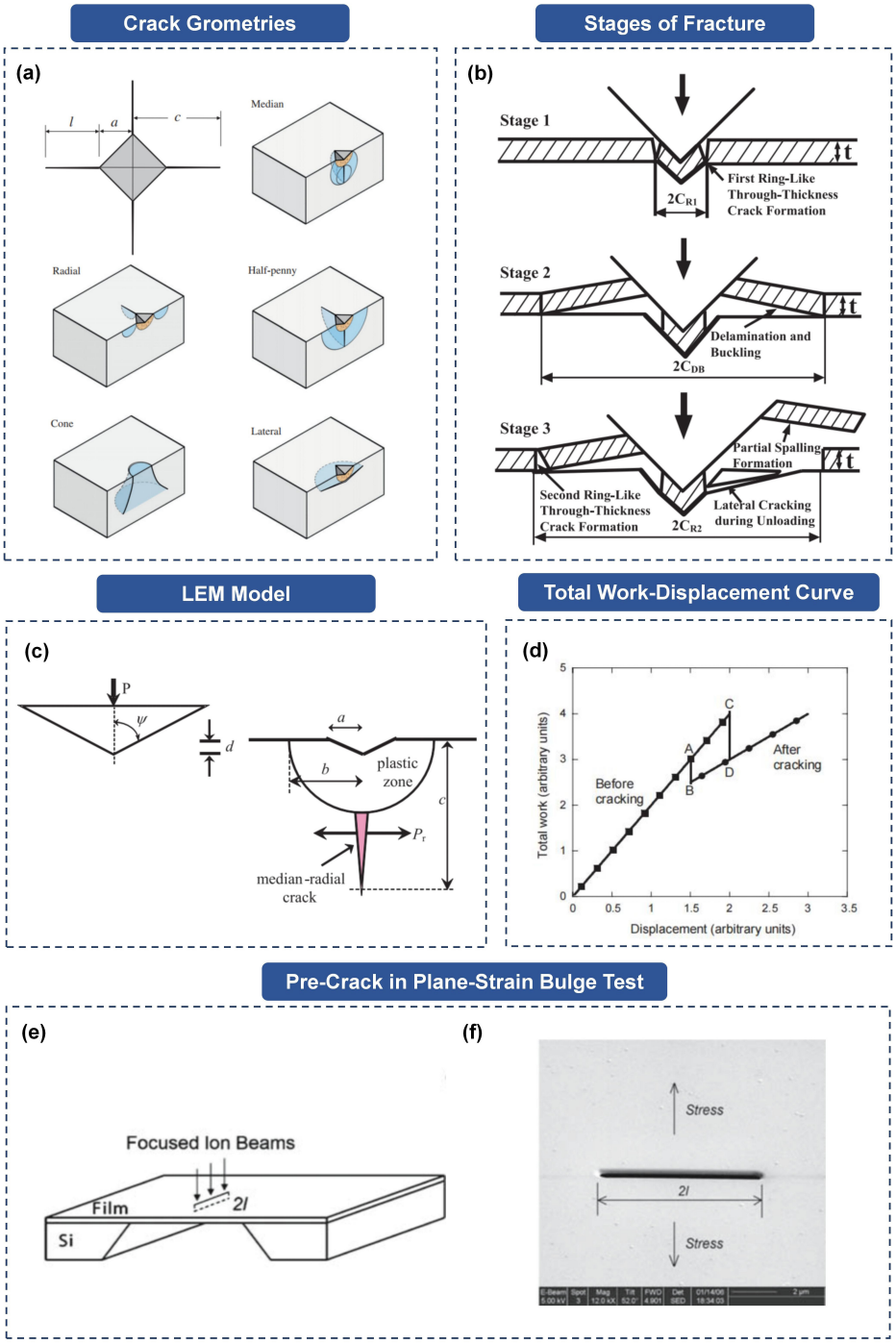

Figure 7. Representative illustration of the measurement of fracture toughness in the nanoindentation test and the bulge test. (a) Possible crack geometries under indentation loading[102]. Copyright (2012), with permission from Elsevier. (b) Schematic diagram of three stages of nanoindentation fracture of thin coating[103]. Copyright (2005), with permission from Elsevier. (c) Schematic of the fracture analysis of the LEM model. P is the load. P_r is wedging force (a pair). a is the contact size. b is the radius of the material. c is the crack size. d is the deflection. ψ is the axis-to-face angle[102]. Copyright (2012), with permission from Elsevier. (d) Schematic total work-displacement curve before and after craking[93]c. Copyright (2006), with permission from Elsevier. (e) Schematic diagram of the microfabrication of a pre-crack located at the central region of a freestanding thin film using a focused ion beam. Reprinted by permission from Springer Nature Customer Service Centre GmbH: Springer Nature, International Journal of Fracture. © 2007. (f) SEM image of a pre-crack. Reprinted by permission from Springer Nature Customer Service Centre GmbH: Springer Nature, International Journal of Fracture. © 2007.

2.3.2 Bulge test

In the bulge test, as shown in Figure 7e, fracture toughness is studied in the bulge test by creating pre-cracks of different lengths, usually with focused ion beams (FIB) or lithography. A SEM image of a typical pre-crack is shown in Figure 7f. The energy release rate G was defined to represent the crack state:

$$G = \frac{\pi\sigma^2 l}{E}\# \quad (17)$$

where σ is the tensile stress, $2l$ is the crack length, and E is the elastic modulus of the film. When G reached the critical energy release rate G_c, the crack expands. Then the critical stress σ_f during the crack propagation is expressed as

$$\sigma_f = \sqrt{\frac{EG_c}{\pi}} l^{-\frac{1}{2}}\# \quad (18)$$

The fracture toughness factor K_{IC} is expressed as

$$K_{IC} = \sigma_f \sqrt{\pi l}\# \quad (19)$$

Based on the above function relationship of pre-crack length and the film's fracture toughness, Xiang et al. obtained the fracture toughness of 150 nm AlTa intermetallic films through the plane-strain bulge test. Merle et al. measured the fracture toughness of low-pressure chemical vapor deposited (LPCVD) silicon nitride films with thicknesses ranging from 40 nm to 108 nm. The obtained fracture toughness was constant across the entire range of thicknesses, proving that the fracture toughness of LPCVD silicon nitride is size-independent. Preiß et al.[104] measured the fracture toughness of Au thin films with thicknesses ranging from 100 to 300 nm fabricated by thermal evaporation. Samples obtained from a single deposition batch were intentionally notched using FIB with gallium, neon, or xenon. The bulge test yielded consistent fracture toughness measurements, regardless of the ion species utilized.

3. Discussion

Measuring the mechanical properties of thin films is crucial for both scientific research and practical applications. However, the excessively low thickness of these films can adversely affect experimental measurements. Consequently, significant efforts have been directed towards experimentally measuring the mechanical properties of thin films, utilizing various techniques to mitigate these effects. Our mini-review primarily concentrates on recent advancements in experimental techniques employed to evaluate the mechanical characteristics of films with thicknesses smaller than the dimensions of a human hair, extending beyond two-dimensional materials. Specifically focusing on measuring the elastic modulus, hardness, strength, and fracture toughness of thin films, we discuss enhanced experimental techniques, including the nanoindentation test, among others. Furthermore, we offer our perspective on potential avenues for future research in this field.

Current techniques for measuring the mechanical properties of thin films demand meticulous sample preparation and intricate experimental setups, yet they encounter persistent challenges. For instance, determining the appropriate indenter and indentation depth in nanoindentation requires careful consideration of factors[18]. such as material properties and surface roughness. Moreover, interfacial damage, such as film delamination around the indenter, could compromise measurement accuracy[95]. Conversely, the mechanical bulking method is highly sensitive to minor fluctuations and exhibits lower precision, while the bulge test is similarly susceptible to pressure fluctuations[72].

New experimental measurements continued to advance the understanding of the mechanical properties of films with thicknesses smaller than ~90 μm, which are intricately linked to various emerging technological applications. Enhanced polyurethane (PU) coatings, refractory high-entropy alloy (RHEA)W-Nb-Mo-Ta-V-O films tailored for the demanding requirements of the aerospace industries[105,106]. Dielectric/metal/dielectric (DMD) multilayered films with sandwich structures, silver nanowires (AgNW) films, poly(3,4-ethylenedioxythiophene): poly(styrene sulfonate) (PEDOT:PSS) films, and $Ti_3C_2T_x$ MXene films find extensive applications in flexible electronics, spanning across various domains such as bioelectronic applications, energy storage devices, and more[107–111]. We anticipate that thin films will continue to have a promising future in various applications.

Looking ahead, several research directions can offer opportunities for the mechanical characterization of thin films. One promising avenue is to apply improved mechanical characterization techniques to a broader range of film types, rather than restricting them to a single type. For instance, while FOW tensile tests are commonly used to measure the mechanical properties

of polymer thin films, if they can be adapted to measure the mechanical properties of other types of films (e.g., metallic films), a wider variety of thin films could be explored, thus advancing their practical applications. Moreover, recent advancements in machine learning (ML) present new opportunities for experimental solid mechanics, encompassing experimental design, data analysis, and more[112]. ML can be utilized to expediently acquire the mechanical properties of thin films. For example, it can analyze the load-displacement curve in nanoindentation test[113] with the specific goal of predicting the mechanical characteristics of thin films. As ML techniques continue to evolve, we anticipate they will significantly aid in characterizing the mechanical properties of thin films in the future.

Acknowledgments

Acknowledge the funding support from the Alliance Foundation of Lanzhou Institute of Chemical Physics, Chinese Academy of Sciences (No. HZJJ22-04).

Ethics Statement

Not applicable.

Consent for publication

Not applicable.

Availability of Supporting Data

Not applicable.

Conflict of Interest

The authors declare that there are no conflicts of interest.

Copyright

References

[1] Borchert JW, Borchert JW, Zschieschang U, et al. Flexible low-voltage high-frequency organic thin-film transistors. *Sci Adv*. 2020;6(21). https://doi.org/10.1126/SCIADV.AAZ5156

[2] Magari Y, Kataoka T, Yeh W, Furuta M. High-mobility hydrogenated polycrystalline In_2O_3 (In_2O_3:H) thin-film transistors. *Nat. Commun*. 2022 13:1. 2022;13(1):1-8. https://doi.org/10.1038/s41467-022-28480-9

[3] Zschieschang U, Waizmann U, Weis J, Borchert JW, Klauk H. Nanoscale flexible organic thin-film transistors. *Sci Adv*. 2022;8(13):9845. https://doi.org/10.1126/SCIADV.ABM9845

[4] Fratelli I, Ciavatti A, Zanazzi E, et al. Direct detection of 5-MeV protons by flexible organic thin-film devices. *Sci Adv*. 2021;7(16):4462-4478. https://doi.org/10.1126/SCIADV.ABF4462

[5] Hellenbrand M, Bakhit B, Dou H, et al. Thin film design of amorphous hafnium oxide nanocomposites enabling strong interfacial resistive switching uniformity. *Sci Adv*. 2023;9(25). https://doi.org/10.1126/SCIADV.ADG1946

[6] Atxabal A, Arnold T, Parui S, et al. Tuning the charge flow between Marcus regimes in an organic thin-film device. *Nat. Commun*. 2019;10(1):1-7. https://doi.org/10.1038/s41467-019-10114-2

[7] Kwon O, Moon S, Yun Y, et al. Highly efficient thin-film 930 nm VCSEL on PDMS for biomedical applications. *Sci. Rep*. 2023;13(1):1-7. https://doi.org/10.1038/s41598-023-27589-1

[8] Balandin AA, Ghosh S, Bao W, et al. Superior thermal conductivity of single-layer graphene. *Nano Lett*. 2008;8(3):902-907. https://doi.org/10.1038/s41598-023-27589-1

[9] Dharmadhikari VS. Characterization of plasma-deposited silicon nitride coating used for integrated circuit encapsulation. *Thin Solid Films*. 1987;153(1-3):459-468. https://doi.org/10.1016/0040-6090(87)90205-7

[10] Oliver WC, Pharr GM. An improved technique for determining hardness and elastic modulus using load and displacement sensing indentation experiments. *J Mater Res*. 1992;7(6):1564-1583. https://doi.org/10.1557/JMR.1992.1564

[11] Jonnalagadda K, Cho SW, Chasiotis I, Friedmann T, Sullivan J. Effect of intrinsic stress gradient on the effective mode-I fracture toughness of amorphous diamond-like carbon films for MEMS. *J Mech Phys Solids*. 2008;56:388-401. https://doi.org/10.1016/j.jmps.2007.05.013

[12] Kim JH, Nizami A, Hwangbo Y, et al. Tensile testing of ultra-thin films on water surface. *Nat. Commun*. 2013;4(1):1-6. https://doi.org/10.1038/ncomms3520

[13] Liu Y, Chen YC, Hutchens S, Lawrence J, Emrick T, Crosby AJ. Directly measuring the complete

stress-Strain response of ultrathin polymer films. *Macromolecules*. 2015;48(18):6534-6540. https://doi.org/10.1021/ACS.MACROMOL.5B01473

[14] Bay RK, Shimomura S, Liu Y, Ilton M, Crosby AJ. Confinement Effect on Strain Localizations in Glassy Polymer Films. *Macromolecules*. 2018;51(10):3647-3653. https://doi.org/10.1021/ACS.MACROMOL.8B00385

[15] Bay RK, Crosby AJ. Uniaxial Extension of ultrathin freestanding polymer films. *ACS Macro Lett*. 2019;8(9):1080-1085. https://doi.org/10.1021/ACSMACROLETT.9B00408

[16] Galuska LA, Muckley ES, Cao Z, et al. SMART transfer method to directly compare the mechanical response of water-supported and free-standing ultrathin polymeric films. *Nat. Commun*. 2021;12(1):1-11. https://doi.org/10.1038/s41467-021-22473-w

[17] Wang G, Hou H, Yan Y, et al. Recent advances in the mechanics of 2D materials. *Int. J. Extreme Manuf*. 2023;5(3). https://doi.org/10.1088/2631-7990/accda2

[18] Jen SU, Wu TC. Young's modulus and hardness of Pd thin films. *Thin Solid Films*. 2005; 492(1-2):166-172. https://doi.org/10.1016/j.tsf.2005.06.048

[19] Lesage J, Pertuz A, Puchi-Cabrera ES, Chicot D. A model to determine the surface hardness of thin films from standard micro-indentation tests. Thin Solid Films. 2005; 492(1-2):232-238. https://doi.org/10.1016/j.tsf.2005.09.194

[20] Bhattacharya AK, Nix WD. Analysis of elastic and plastic deformation associated with indentation testing of thin films on substrates. *Int J Solids SlrUClures*. 1988;24(12):1287-1298. https://doi.org/10.1016/0020-7683(88)90091-1

[21] Gao Y, Kim S, Zhou S, et al. Elastic coupling between layers in two-dimensional materials. *Nat Mater*. 2015;14(7):714-720. https://doi.org/10.1038/nmat4322

[22] Hertz H. Ueber die Berührung fester elastischer Körper. *Journal für die reine und angewandte Mathematik*.1882;(92):156-171. https://doi.org/10.1515/CRLL.1882.92.156

[23] Johnson Kenneth Langstreth , Kendall Kevin and Roberts A. D. Surface energy and the contact of elastic solids. *Proc. R. Soc. Lond*. 1971;324(1558):301-313. https://doi.org/10.1098/rspa.1971.0141

[24] Derjaguin B V., Muller VM, Toporov YP. Effect of contact deformations on the adhesion of particles. *J Colloid Interface Sci*. 1975;53(2):314-326. https://doi.org/10.1016/0021-9797(75)90018-1

[25] Zhao BX, Arunbabu D, McDonald B. Polymers, Adhesion, and Paper Materials. 2013, 501-543. https://doi.org/10.1002/9781118505175.ch12

[26] Jönsson B, Hogmark S. Hardness measurements of thin films. *Thin Solid Films*. 1984;114(3):257-269. https://doi.org/10.1016/0040-6090(84)90123-8

[27] Doerner MF, Nix WD. A method for interpreting the data from depth-sensing indentation instruments. *J Mater Res*. 1986;1(4):601-609. https://doi.org/10.1557/JMR.1986.0601

[28] King RB. Elastic analysis of some punch problems for a layered medium. *Int J Solids Struct*. 1987;23(12):1657-1664. https://doi.org/10.1016/0020-7683(87)90116-8

[29] Saha R, Nix WD. Effects of the substrate on the determination of thin film mechanical properties by nanoindentation. *Acta Mater*. 2002;50(1):23-38. https://doi.org/10.1016/S1359-6454(01)00328-7

[30] Huajian G, Cheng-Hsin C, Jin L. Elastic contact versus indentation modeling of multi-layered materials. *Int J Solids Struct*. 1992;29(20):2471-2492. https://doi.org/10.1016/0020-7683(92)90004-D

[31] Zhou XY, Jiang ZD, Wang HR, Zhu Q. A Method to extract the intrinsic mechanical properties of soft metallic thin films based on nanoindentation continuous stiffness measurement technique. *J Phys Conf Ser*. 2006;48(1):1096. https://doi.org/10.1088/1742-6596/48/1/204

[32] Zhou B, Prorok BC. A discontinuous elastic interface transfer model of thin film nanoindentation. *Exp Mech*. 2010;50(6):793-801. https://doi.org/10.1007/s11340-009-9309-7

[33] Ma Y, Wang R cong, Xie X you. Influence of oxygen flow rate and annealing temperature on composition, microstructure and mechanical properties of Fe–O films by reactive magnetron sputtering. *Vacuum*. 2022;205:111426. https://doi.org/10.1016/j.vacuum.2022.111426

[34] Lekoui F, Hassani S, Amrani R, et al. Investigation of the deposition time effect on the structural, morphological, and mechanical properties of TiAlN protective thin films. *Braz. J. Phys*. 2022;52(6). https://doi.org/10.1007/s13538-022-01200-w

[35] Kim K, Park S, Kim T, Park Y, Sim GD, Lee D. Mechanical, electrical properties and microstructures of combinatorial Ni-Mo-W alloy films. *J. Alloys Compd*. 2022;919:165808. https://doi.org/10.1016/j.jallcom.2022.165808

[36] Boughrara N, Benzarti Z, Khalfallah A, Oliveira JC, Evaristo M, Cavaleiro A. Thickness-dependent physical and nanomechanical properties of $Al_xGa_{1-x}N$ thin films. Mater. Sci. Semicond. Process. 2022;151:107023 https://doi.org/10.1016/j.mssp.2022.107023

[37] Manica D, Ion V, Sopronyi M, Andrei F, Bonciu A, Scarisoreanu N. Mechanical properties characterization for thin layers oxide (Al_2O_3), deposited by PLD-large area. *Appl Phys A Mater Sci Process*. 2022;128(11). https://doi.org/10.1007/s00339-022-06098-4

[38] Hsiao CC, Yu SY, Maruyama K, Kawakami Y, Narita F. cite this article: Kohei Maruyama et al. *Jpn. J. Appl. Phys*. 2022;61:1011. https://doi.org/10.35848/1347-4065/ac7d96

[39] Dziri A, Montagne A, Roudet F, Ziouche K, Chicot D. Martens hardness of constantan thin films on (100) Si wafer: Improvement in contact area function in nanoindentation. *Thin Solid Films*. 2023;768. https://doi.org/10.1016/j.tsf.2023.139712

[40] Valour A, Higuita MAU, Guillonneau G, et al. Optical, electrical and mechanical properties of TiN thin film obtained from a TiO_2 sol-gel coating and rapid thermal nitridation. *Surf Coat Technol*. 2021;413. https://doi.org/10.1016/j.surfcoat.2021.127089

[41] Yang L, Chen Y, Xu Z, Toshiaki N, Xi Y, Ni Q. Effect of heat treatment on mechanical property of amorphous carbon films by magnetron sputtering. *Diam Relat Mater*. 2022;129. https://doi.org/10.1016/j.diamond.2022.109328

[42] Components P& MTSocietyTC, Institute of Electrical and Electronics Engineers, IMAPS All Asia Conference. 11th International Microsystems, Packaging, Assembly and Circuits Technology Conference (IMPACT 2016) : Proceedings : October 26-28, 2016, Taipei.

[43] Li R, Li Y, Yan C, et al. Thickness-dependent and tunable mechanical properties of $CaTiO_3$ dielectric thin films determined by nanoindentation technique. *Ceram Int*. 2020;46(14):22643-22649. https://doi.org/10.1016/j.ceramint.2020.06.027

[44] Garcia R. Nanomechanical mapping of soft materials with the atomic force microscope: Methods, theory and applications. *Chem Soc Rev*. 2020;49(16):5850-5884. https://doi.org/10.1039/d0cs00318b

[45] Park JY, Kwon S, Kim JH. Nanomechanical and charge transport properties of two-dimensional atomic sheets. *Adv Mater Interfaces*. 2014;1(3). https://doi.org/10.1002/admi.201300089

[46] Cortelli G, Patruno L, Cramer T, Murgia M, Fraboni B, De Miranda S. Atomic force microscopy nanomechanics of hard nanometer-thick films on soft substrates: insights into stretchable conductors. *ACS Appl Nano Mater*. 2021;4(8):8376-8382. https://doi.org/10.1021/acsanm.1c01590

[47] Lee D, Barber JR, Thouless MD. Indentation of an elastic half space with material properties varying with depth. *Int J Eng Sci*. 2009;47(11-12):1274-1283. https://doi.org/10.1016/j.ijengsci.2008.08.005

[48] Printz AD, Zaretski A V., Savagatrup S, Chiang ASC, Lipomi DJ. Yield point of semiconducting polymer films on stretchable substrates determined by onset of buckling. *ACS Appl Mater Interfaces*. 2015;7(41):23257-23264. https://doi.org/10.1021/ACSAMI.5B08628

[49] Huang H, Spaepen F. Tensile testing of free-standing Cu, Ag and Al thin films and Ag/Cu multilayers. *Acta Mater*, 2000;48(12): 3261-3269. doi.org/10.1016/S1359-6454(00)00128-2

[50] Amherst S, Dissertations D, Huang J. Wrinkling Of Floating Thin Polymer Films. *Doctoral Dissertations*. 1896. https://doi.org/10.7275/5671733

[51] Koo J, Lee S, Kim J, et al. Evaluating mechanical properties of 100nm-thick atomic layer deposited Al_2O_3 as a free-standing film. *Scr Mater*. 2020; 187:256-261.

https://doi.org/10.1016/j.scriptamat.2020.06.028

[52] Zhang S, Ocheje MU, Luo S, et al. Probing the viscoelastic property of pseudo free-standing conjugated polymeric thin films. *Macromol Rapid Commun*. 2018;39(14). https://doi.org/10.1002/MARC.201800092

[53] Zhang H, Sakagami D, Huang W, Kimura H, Okamura Y. Measurement and modelling of tensile moduli of polymer blend thin films with phase separated structures. *Polymer* (*Guildf*). 2020;190. https://doi.org/10.1016/j.polymer.2020.122233

[54] Saito M, Ito K, Yokoyama H. Mechanical properties of ultrathin polystyrene-b-polybutadiene-b-polystyrene block copolymer films: film thickness-dependent young's modulus. *Macromolecules*. 2021;54(18):8538-8547. https://doi.org/10.1021/acs.macromol.1c01406

[55] Saito M, Ito K, Yokoyama H. Film thickness and strain rate dependences of the mechanical properties of polystyrene-b-polyisoprene-b-polystyrene block copolymer ultrathin films forming a spherical domain. *Polymer* (*Guildf*). 2022;258. https://doi.org/10.1016/j.polymer.2022.125302

[56] Kim YU, Ma BS, Kim Y, et al. Comparison of the mechanical properties of polymer blend and main-chain conjugated copolymer films with donor–acceptor heterojunctions. *Chem. Eng. J*. 2021;415. https://doi.org/10.1016/j.cej.2021.128952

[57] Oh SJ, Ma BS, Yang C, Kim TS. Intrinsic mechanical properties of free-standing SiN_x thin films depending on PECVD conditions for controlling residual stress. *ACS Appl Electron Mater*. 2022;4(8):3980-3987. https://doi.org/10.1021/acsaelm.2c00623

[58] Keren S, Bukowski C, Barzilay M, et al. Mechanical behavior of hybrid thin films fabricated by sequential infiltration synthesis in water-rich environment. *ACS Appl Mater Interfaces*. 2023;15(40):47487-47496. https://doi.org/10.1021/acsami.3c09609

[59] Zhang S, Koizumi M, Cao Z, et al. Directly probing the fracture behavior of ultrathin polymeric films. *ACS Polymers Au*. 2021;1(1):16-29. https://doi.org/10.1021/acspolymersau.1c00005

[60] Kim KH, Jeong S, Kim HJ. Numerical and experimental analyses of the crack propagation in nanocomposite thin-films by using dynamic particle difference methods. *Polymer* (*Guildf*). 2022;240. https://doi.org/10.1016/j.polymer.2022.124527

[61] Pei D, An C, Zhao B, et al. Polyurethane-based stretchable semiconductor Nanofilms with High Intrinsic Recovery Similar to Conventional Elastomers. *ACS Appl Mater Interfaces*. Published online 2022. https://doi.org/10.1021/acsami.2c07445

[62] Beams J W, Walker W E, Morton Jr H S. Mechanical properties of thin films of silver. *Phys. Rev*. 1952, 87(3): 524-552. https://doi.org/10.1103/PhysRev.87.524.2

[63] Xiang Y, Chen X, Vlassak JJ. Plane-strain bulge test for thin films. *J Mater Res*. 2005;20(9):2360-2370. https://doi.org/10.1557/JMR.2005.0313

[64] Vlassak JJ, Nix WD. A new bulge test technique for the determination of Young's modulus and Poisson's ratio of thin films. *J Mater Res*. 1992;7(12):3242-3249. https://doi.org/10.1557/JMR.1992.3242

[65] Kalkman AJ, Verbruggen AH, Janssen GCAM, Groen FH. A novel bulge-testing setup for rectangular free-standing thin films. *Rev. Sci. Instrum*. 1999;70(10):4026-4031. https://doi.org/10.1063/1.1150029

[66] Small MK, Nix WD. Analysis of the accuracy of the bulge test in determining the mechanical properties of thin films. *J Mater Res*. 1992;7(6): 1553-1563. https://doi.org/10.1557/JMR.1992.1553

[67] Pinyen Lin. The in-situ measurement of mechanical properties of multi-layer coatings. 1990. https://dspace.mit.edu/handle/1721.1/14102

[68] Rontu V, Nolvi A, Hokkanen A, Haeggström E, Kassamakov I, Franssila S. Elastic and fracture properties of free-standing amorphous ALD Al_2O_3 thin films measured with bulge test. *Mater Res Express*. 2018;5(4). https://doi.org/10.1088/2053-1591/aabbd5

[69] Mongkolsuttirat K, Smyth JR, McLean M, Brown WL, Vinci RP. The effects of solid solution and oxide dispersion alloying on the viscoelastic behavior of Au alloy thin films. *Acta Mater*.

2019;168:275-286.
https://doi.org/10.1016/j.actamat.2019.02.023

[70] Tinoco HA, Holzer J, Pikálek T, et al. Determination of elastic parameters of Si_3N_4 thin films by means of a numerical approach and bulge tests. *Thin Solid Films*. 2019;672:66-74.
https://doi.org/10.1016/j.tsf.2018.12.039

[71] Österlund E, Kinnunen J, Rontu V, Torkkeli A, Paulasto-Kröckel M. Mechanical properties and reliability of aluminum nitride thin films. *J Alloys Compd*. 2019;772:306-313.
https://doi.org/10.1016/j.jallcom.2018.09.062

[72] Montinaro N, Lo Cicero U, D'Anca F, Bozzo E, Paltani S, Barbera M. Elastic characterization of nanometer-thick polymeric film for astrophysics application with an experimental-numerical method. *J Astron Telesc Instrum Syst*. 2023;9(03).
https://doi.org/10.1117/1.jatis.9.3.034005

[73] Stafford CM, Harrison C, Beers KL, et al. A buckling-based metrology for measuring the elastic moduli of polymeric thin films. *Nat Mater*. 2004;3(8):545-550.
https://doi.org/10.1038/nmat1175

[74] Khang DY, Rogers JA, Lee HH. Mechanical buckling: Mechanics, metrology, and stretchable electronics. *Adv Funct Mater*. 2009;19(10):1526-1536.
https://doi.org/10.1002/adfm.200801065

[75] Rencheck ML, Rodriguez R, Miller NA, Davis CS. A buckling mechanics approach to elastic modulus determination of glassy polymer films. *J Polym Sci B Polym Phys*. 2019;57(1):15-20.
https://doi.org/10.1002/polb.24755

[76] Lee J, Park J, Yoo D, et al. High uniaxial buckling strain for measuring the mechanical properties of nanoporous gold films. *Scr Mater*. 2021;197.
https://doi.org/10.1016/j.scriptamat.2021.113816

[77] Stimpson TC, Osorio DA, Cranston ED, Moran-Mirabal JM. Direct comparison of three buckling-based methods to measure the elastic modulus of nanobiocomposite thin films. *ACS Appl Mater Interfaces*. 2021;13(24):29187-29198.
https://doi.org/10.1021/acsami.1c08056

[78] Niinivaara E, Desmaisons J, Dufresne A, Bras J, Cranston ED. Film thickness limits of a buckling-based method to determine mechanical properties of polymer coatings. *J Colloid Interface Sci*. 2021;582:227-235.
https://doi.org/10.1016/j.jcis.2020.08.025

[79] Rencheck ML, Weiss AJ, El Awad Azrak SM, et al. Nanocellulose film modulus determination via buckling mechanics approaches. *ACS Appl Polym Mater*. 2020;2(2):578-584.
https://doi.org/10.1021/acsapm.9b00969

[80] Vannozzi L, Gouveia P, Pingue P, Canale C, Ricotti L. Novel ultrathin films based on a blend of PEG- b-PCL and PLLA and doped with ZnO nanoparticles. *ACS Appl Mater Interfaces*. 2020;12(19):21398-21410.
https://doi.org/10.1021/acsami.0c00154

[81] Ebadi-Jamkhaneh M, Kontoni D P N, Ahmadi M. Evaluation of the Behavior of Gusset Plates in Concentrically Braced Steel Frames Under Cyclic Loading//Recent Trends in Civil Engineering: Select Proceedings of ICRACE 2021. Singapore: Springer Nature Singapore, 2022: 371-387.

[82] Murthy D N P, Xie M, Jiang R. Weibull models. John Wiley & Sons, 2004.

[83] Borrero-Lopez O, Hoffman M. Measurement of fracture strength in brittle thin films. *Surf Coat Technol*. 2014;254:1-10.
https://doi.org/10.1016/j.surfcoat.2014.05.053

[84] Li P, Cao K, Jiang C, et al. In situ tensile fracturing of multilayer graphene nanosheets for their in-plane mechanical properties. *Nanotechnology*. 2019;30(47).
https://doi.org/10.1088/1361-6528/ab3cd3

[85] Jen MHR, Wu YH, Liou TY. Mechanical behavior of thin films due to in-plane tensile and fatigue loadings. *AIP Adv*. 2019;9(5).
https://doi.org/10.1063/1.5088848

[86] Min HG, Kang DJ, Park JH. Comparison of tensile and fatigue properties of copper thin film depending on process method. *Appl. Sci*. (*Switzerland*). 2020;10(1).
https://doi.org/10.3390/app10010388

[87] Berlia R, Rasmussen P, Yang S, Rajagopalan J. Tensile behavior and inelastic strain recovery of Cu-Co nanolaminates. *Scr Mater*. 2021;197.
https://doi.org/10.1016/j.scriptamat.2021.113781

[88] Javed H, Merle B, Preiß E, Hivet R, Benedetto A, Göken M. Mechanical characterization of metallic thin films by bulge and scratch testing. *Surf Coat Technol*. 2016;289:69-74.

https://doi.org/10.1016/j.surfcoat.2016.01.051

[89] Tinoco HA, Holzer J, Pikálek T, et al. Determination of the yield stress in Al thin film by applying bulge test. In: *Journal of Physics: Conference Series*. Vol 1777. IOP Publishing Ltd; 2021. https://doi.org/10.1088/1742-6596/1777/1/012030

[90] Gusev EE, Tovarnov DA, Dedkova AA, Onufrienko AP, Djuzhev NA. Experimental Study mechanical stresses and Strength in multilayer PECVD SiO_2. In: *Proceedings of the* 2021 *IEEE Conference of Russian Young Researchers in Electrical and Electronic Engineering, ElConRus* 2021. Institute of Electrical and Electronics Engineers Inc.; 2021:2437-2441. https://doi.org/10.1109/ElConRus51938.2021.9396248

[91] Li X, Diao D, Bhushan B. Fracture mechanisms of thin amorphous carbon films in nanoindentation. *Acta Mater*, 1997, 45(11): 4453-4461. doi.org/10.1016/S1359-6454(97)00143-2

[92] Den Toonder J, Malzbender J, De With G, Balkenende R. Fracture toughness and adhesion energy of sol-gel coatings on glass. *J Mater Res*. 2002;17(1):224-233. https://doi.org/10.1557/JMR.2002.0032

[93] Chen J, Bull SJ. Assessment of the toughness of thin coatings using nanoindentation under displacement control. In: *Thin Solid Films*. 2006;494:1-7. https://doi.org/10.1016/j.tsf.2005.08.176

[94] Malzbender J, De With G. Energy Dissipation, Fracture toughness and the indentation loaddisplacement curve of coated materials. *Surf. Coat. Technol*. 2000; 135 (1): 60-68. https://doi.org/10.1016/S0257-8972(00)00906-3

[95] *EPTC :* 2017 *IEEE* 19*th Electronics Packaging Technology Conference :* 6-9 *December* 2017.

[96] Chen J, Bull SJ. Indentation fracture and toughness assessment for thin optical coatings on glass. *J Phys D Appl Phys*. 2007;40(18):5401-5417. https://doi.org/10.1088/0022-3727/40/18/S01

[97] Cheng W, Li W, Wang J, et al. Effects of N_2/Ar flow ratio on the structures and mechanical behavior of ZrO_xN_y/V_2O_3 nano-multilayered films. *Mater. Sci. Eng. A*. 2022;849. https://doi.org/10.1016/j.msea.2022.143419

[98] Soler R, Gleich S, Kirchlechner C, Scheu C, Schneider JM, Dehm G. Fracture toughness of Mo2BC thin films: Intrinsic toughness versus system toughening. *Mater Des*. 2018;154:20-27. https://doi.org/10.1016/j.matdes.2018.05.015

[99] Pradeepkumar MS, Sibin KP, Hasan MA, Dey A, Mukhopadhyay AK. Nanoindentation based fracture studies of ITO coating. *Ceram Int*. 2021;47(10):14717-14722. https://doi.org/10.1016/j.ceramint.2021.01.005

[100] Jiang ZT, Lei MK. Structure and fracture toughness of TiAlN thin films deposited by deep oscillation magnetron sputtering. *Thin Solid Films*. 2022;754. https://doi.org/10.1016/j.tsf.2022.139306

[101] Wang Z, Zhang M, Zhao J, Zhao H. Cyclic nanoindentation of ITO/Ag/ITO multilayer films: Hysteresis behavior and cyclic deformation response. *Ceram Int*. 2022;48(14):21054-21059. https://doi.org/10.1016/j.ceramint.2022.04.150

[102] Lee JH, Gao YF, Johanns KE, Pharr GM. Cohesive interface simulations of indentation cracking as a fracture toughness measurement method for brittle materials. *Acta Mater*. 2012;60(15):5448-5467. https://doi.org/10.1016/j.actamat.2012.07.011

[103] Zhang S, Sun D, Fu Y, Du H. Toughness measurement of thin films: A critical review. *Surf Coat Technol*. 2005;198(1-3 SPEC. ISS.):74-84. https://doi.org/10.1016/j.surfcoat.2004.10.021

[104] Preiß EI, Merle B, Xiao Y, et al. Applicability of focused Ion beam (FIB) milling with gallium, neon, and xenon to the fracture toughness characterization of gold thin films. *J Mater Res*. 2021;36(12):2505-2514. https://doi.org/10.1557/s43578-020-00045-w

[105] Xavier JR. Multilayered nanocomposite coatings for enhanced anticorrosive, flame retardant, and mechanical properties in automobile and aerospace industries. *J Appl Polym Sci*. 2023;140(24). https://doi.org/10.1002/app.53943

[106] Liao WB, Xu CH, Wang TL, Feng CS, Khan MA, Yasin G. Oxidation influences on the microstructure and mechanical properties of W–Nb–Mo–Ta–V–O refractory high-entropy alloy films. *Vacuum*. 2023;207. https://doi.org/10.1016/j.vacuum.2022.111586

[107] Park YB, Lee S, Tobah M, Ma T, Guo LJ. Optimized optical/electrical/mechanical properties

of ultrathin metal films for flexible transparent conductor applications: review. *Opt Mater Express*. 2023;13(2):304. https://doi.org/10.1364/ome.473277

[108]Kwon J, Suh YD, Lee J, et al. Recent progress in silver nanowire based flexible/wearable optoelectronics. *J Mater Chem C Mater*. 2018;6(28): 7445-7461. https://doi.org/10.1039/c8tc01024b

[109]Lee S, Guo LJ. Bioinspired toughening mechanisms in a multilayer transparent conductor structure. *ACS Appl. Mater. Interfaces*. 2022;14(5):7440-7449. https://doi.org/10.1021/acsami.1c21923

[110]Won, Daeyeon, et al. Digital selective transformation and patterning of highly conductive hydrogel bioelectronics by laser-induced phase separation. *Sci Adv*. 2022; 8(23). https://doi.org/ 10.1126/sciadv.abo3209

[111]Wang J, Jiang D, Zhang M, et al. Ice crystal-assisted intercalation of PANI within $Ti_3C_2T_x$ MXene thin films for flexible supercapacitor electrodes with simultaneously high mechanical strength and rate performance. *J Mater Chem A Mater*. 2022;11(3):1419-1429. https://doi.org/10.1039/d2ta08176h

[112]Jin H, Zhang E, Espinosa HD. Recent advances and applications of machine learning in experimental solid mechanics: a review. *Appl. Mech. Rev*. 2023;75(6):061001. https://doi.org/10.1115/1.4062966

[113]Long X, Lu C, Shen Z, Su Y. Identification of Mechanical Properties of Thin-Film Elastoplastic Materials by Machine Learning. *Acta Mech. Solida Sin*. 2023;36(1):13-21. https://doi.org/10.1007/s10338-022-00340-5